Acta Pharmaceutica Sinica B 2024;14(10):4413–4430

Chinese Pharmaceutical Association
Institute of Materia Medica, Chinese Academy of Medical Sciences

Acta Pharmaceutica Sinica B

www.elsevier.com/locate/apsb
www.sciencedirect.com

ORIGINAL ARTICLE

PGC-1α-mediated imbalance of mitochondria-lipid droplet homeostasis in neomycin-induced ototoxicity and nephrotoxicity

Bin Chen [a,†], Cheng Cheng [b,c,†], Yunhao Wu [d,e,†], Siyu Li [b,†], Mo Han [a], Le Zhen [a], Ying Peng [a], Suhan Guo [a], Kaidi Shen [a], Xia Gao [b], Renjie Chai [e,c,f,*], Guangji Wang [a,*], Fang Zhou [a,*]

[a]*Key Laboratory of Drug Metabolism and Pharmacokinetics, State Key Laboratory of Natural Medicines, China Pharmaceutical University, Nanjing 210009, China*
[b]*Department of Otolaryngology Head and Neck Surgery, Nanjing Drum Tower Hospital, Affiliated Hospital of Medical School, Nanjing University, Nanjing 210096, China*
[c]*Co-Innovation Center of Neuroregeneration, Nantong University, Nantong 226001, China*
[d]*Medical Science and Technology Innovation Center, Shandong First Medical University & Shandong Academy of Medical Sciences, Jinan 250117, China*
[e]*State Key Laboratory of Digital Medical Engineering, Department of Otolaryngology Head and Neck Surgery, Zhongda Hospital, School of Life Sciences and Technology, Advanced Institute for Life and Health, Jiangsu Province High-Tech Key Laboratory for Bio-Medical Research, Southeast University, Nanjing 210096, China*
[f]*Department of Neurology, Aerospace Center Hospital, School of Life Science, Beijing Institute of Technology, Beijing 100081, China*

Received 25 January 2024; received in revised form 23 March 2024; accepted 24 April 2024

KEY WORDS

Mitochondria;
Neomycin;
Nephrotoxicity;
Ototoxicity;

Abstract Ototoxicity and nephrotoxicity are the most prevalent side effects of aminoglycoside antibiotics (gentamicin, amikacin, neomycin) and platinum anti-tumor drugs (cisplatin, carboplatin). The inner ear and kidney share similarities in drug deposition and toxicity, but the underlying pathophysiological mechanisms remain unclear. Investigating the shared mechanisms and metabolic alterations in these distinct organs will provide valuable insights for clinical therapy. A strong correlation

*Corresponding authors.
E-mail addresses: zf1113@163.com (Fang Zhou), guangjiwang@hotmail.com (Guangji Wang), renjiec@seu.edu.cn (Renjie Chai).
†These authors made equal contributions to this work.
Peer review under the responsibility of Chinese Pharmaceutical Association and Institute of Materia Medica, Chinese Academy of Medical Sciences.

https://doi.org/10.1016/j.apsb.2024.05.024

Lipid metabolism;
Triacylglycerol;
PGC-1α;
PLIN3

has been identified between the spatiotemporal accumulation patterns of neomycin and the specific occurrence of lipid metabolism disorders in these two organs. The primary allocation of neomycin to mitochondria results in a notable escalation in the accumulation of lipid droplets (LDs) and more interactions between mitochondria and LDs, leading to a sequence of disturbances in lipid metabolism, such as increased lipid ROS and the blocked transfer of fatty acids from LDs to mitochondria. PGC-1α deficiency worsens the neomycin-induced disorders in lipid metabolism and intensifies the pathological interactions between mitochondria and LDs, as indicated by the exacerbated disturbance of dynamic LD turnover, increased level of oxidized lipids and decreased use of fatty acids. This investigation provides a fresh perspective on the lipid metabolic dysfunction related to mitochondria−LD interactions in drug-induced ototoxicity and nephrotoxicity, potentially providing novel avenues for intervention strategies.

1. Introduction

Hearing impairment is frequently observed in individuals with renal failure, although the relationship between the auditory system and the kidneys remains unclear. Studies conducted on patients with chronic kidney disease (CKD) have demonstrated that approximately 20% to 77% of these individuals experience some degree of hearing impairment, ranging from mild to moderate to severe[1,2]. Notably, a recent investigation revealed that the CKD group exhibited a higher prevalence of sudden sensorineural hearing loss compared to the control group, with incidence rates of 2.16 and 1.74 per 1000 person-years, respectively[3]. According to the tenets of Traditional Chinese Medicine, the kidney assumes a vital role in auditory function due to its purported association with the ears, and the nourishment of the kidney through essential qi is advantageous for hearing function[4]. Additionally, the inner ear and kidney exhibit many similarities in drug deposition and toxic responses[5]. It is noteworthy that specific clinical agents, including aminoglycosides (AGs) and platinum-based chemotherapeutic agents, possess the capacity to induce concurrent hearing loss and renal impairment[6]. AGs, either used alone or in combination with β-lactams and other antibacterial agents, are frequently utilized for the treatment of severe infectious diseases, particularly those caused by Gram-negative aerobes or drug-resistant bacteria[7]. The bactericidal activity of AGs is acknowledged to be contingent upon concentration[8]. Nevertheless, the administration of AGs is significantly limited by the potential for dose-related nephrotoxicity and ototoxicity, which can result in compromised treatment outcomes and patient prognosis[9]. Consequently, the prevention and mitigation of nephrotoxicity and ototoxicity associated with AGs and platinum-based drugs represent a pressing concern in clinical practice.

Our previous studies have demonstrated a positive correlation between the toxicity levels of AGs (gentamicin, amikacin and etimicin) and their accumulation in the kidneys and inner ears, particularly within the mitochondria of hair cells and renal tubular epithelial cells[10]. Similarly, cisplatin has been observed to selectively accumulate in mitochondria, resulting in toxicity through binding to mitochondrial DNA in renal tubular epithelial cells[11-13]. The abundance of mitochondria in both renal proximal tubular epithelial cells and cochlear hair cells is attributed to their need for substantial energy to support cellular functions[14,15]. Mitochondria play a vital role in the oxidation of fatty acids and the production of energy[16]. However, the specific alterations in mitochondria-mediated energy metabolism and the underlying mechanism of drug-induced renal injury and hearing impairment remain undisclosed.

Lipids serve as the primary source of energy in kidney proximal tubular cells, and disruptions in lipid metabolism have been implicated in various kidney diseases[17-19]. Xu et al.[20] have substantiated that cisplatin-induced lipid accumulation and impairment of fatty acid oxidation (FAO) contribute to kidney injury. Sun et al.[21] reported that the consumption of a high-fat diet resulted in kidney injury through the exacerbation of lipid accumulation, oxidative stress, inflammatory response, and mitochondrial damage. However, the relationship between lipid metabolism and hearing function remains largely unexplored. Prior investigations conducted on clinical human cohorts have indicated that triacylglycerol (TAG) has been identified as a risk factor for sudden sensorineural hearing loss, with individuals exhibiting elevated plasma TAG levels being particularly vulnerable to hearing impairment when exposed to noise[22,23]. Furthermore, mitochondria, which function as vital sites for lipid metabolism, have a significant impact on maintaining cellular energy supply and managing oxidative stress. The connectedness between mitochondria and lipid droplets (LDs) metabolism has been linked to the development of various diseases[24]. Nevertheless, the alterations in lipid metabolism and the interplay between mitochondria and lipid homeostasis in neomycin-induced concurrent hearing and kidney injury remain poorly understood.

To investigate the common mechanism responsible for neomycin-induced hearing and kidney injury, a mouse model was established using neomycin to induce concurrent hearing and renal injury. Neomycin Texas-red conjugate (NTR) imaging and HPLC−MS/MS quantitative analysis were employed to reveal the spatiotemporal distribution patterns of neomycin *in vitro* and *in vivo*, and to determine its correlation with hearing and kidney injury. By analyzing the spatiotemporal distribution characteristics of neomycin in these two organs, the significant involvement of mitochondria-lipid metabolism disorder in neomycin-induced toxicity was elucidated, focusing on lipid and energy metabolism.

2. Materials and methods

2.1. Animals and treatment

WT FVB mice of both sexes were treated with 200 mg/kg neomycin (Sigma−Aldrich, St. Louis, MO, USA) or neomycin

Texas-red conjugate (NTR) subcutaneously from P8 (postnatal Day 8) to P14 for 7 consecutive days. After neomycin treatment, neonatal mice were euthanized 24 h after weaning to collect tissues for experimental detection. FVB mice were purchased from Beijing Vital River Laboratory Animal Technology Co., Ltd. (Beijing, China).

PGC-1α whole-body knockout (KO) animals of both sexes were purchased from Cyagen (Cyagen, Santa Clara, CA, USA). Briefly, mouse *Pgc-1α* gene (GenBank accession number: NM_008904.2; Ensembl: ENSMUSG00000029167) is located on mouse chromosome 5. Among the 13 identified exons, the ATG start codon is located in exon 1, and the TAA stop codon is located in exon 13. Exons 3 to 7 are selected as target sites. Two pairs of gRNA targeting vectors were constructed and sequence confirmed. Cas9 mRNA and gRNA were injected together into mice to generate targeted knockout offspring. F0 generation animals were identified by PCR and then subjected to sequence analysis. They were subsequently mated with wild-type mice to test germline transmission and to generate F1 animals. The genotype of the offspring mice was confirmed using nucleic acid gel electrophoresis. WT or PGC-1α KO mice were treated with 100 mg/kg neomycin from P8 to P14 for 7 consecutive days.

All the animal methods were conducted in accordance with the National Institutes of Health Guide for the Care and Use of Laboratory Animals and were approved by the Ethics Committee on Animal Experimentation of China Pharmaceutical University (Nanjing, China).

2.2. Auditory brain response (ABR) test

The hearing thresholds of mice were measured with the ABR test. Mice were anesthetized with ketamine (100 mg/kg) and xylazine (25 mg/kg) and placed on a thermostatic heating pad in a sound-attenuating chamber to maintain body temperature. Six frequencies (4, 8, 12, 16, 24 and 32 kHz) were assessed with a TDT system 3 (Tucker-Davies Technologies, Gainesville, FL, USA) as previously described[25].

2.3. Cochlear dissection and immunostaining

Neomycin- or saline-treated mice were decapitated at P15, after which the otic capsules were isolated. For the organ of Corti, cochleae were transferred into PBS and micro-dissected under a microscope following 4% paraformaldehyde (PFA) fixation and 0.5 M EDTA calcification. After removing the capsules and modiolus, three turns of Corti were placed flat on 10 mm round coverslips coated with Cell-Tak (Corning, Corning, NY, USA) for further immunostaining.

The sections were immersed in blocking solution (0.1% Triton X-100, 5% donkey serum, 1% BSA in PBS) for 1 h to eliminate nonspecific binding. The membranes were then incubated with primary antibodies against MYO7A (1:400, Proteus Biosciences Inc, Waltham, MA, USA) diluted in blocking solution at 4 °C overnight. After that, samples were washed with PBS and incubated with the corresponding secondary antibody (1:1000, Invitrogen, Carlsbad, CA, USA) diluted in PBS with 0.1% Triton X-100 and 1% BSA at room temperature (RT) for 1 h. The secondary antibodies were removed, and the samples were incubated with DAPI (Beyotime, Shanghai, China) or phalloidin (Thermo Fisher Scientific, Waltham, MA, USA) for 30 min at RT. After washing with PBS, the sections were covered with an anti-fade mounting medium and observed under a laser scanning confocal microscope (Olympus Corporation, Tokyo, Japan).

2.4. Bodipy(493/503), Bodipy(581/591)-C11, Bodipy(558/568)-C12, and Mitotracker staining

Bodipy(493/503) (Invitrogen) was used as a stain for LDs. Bodipy(581/591)-C11 (Invitrogen) was used to detect lipid peroxidation. Bodipy(558/568)-C12 (Invitrogen) was used to track fatty acids uptake and location. Tissue sections were stained with 1 μmol/L Bodipy(493/503). Nuclei were stained with DAPI. For cell staining, cells were cultured with a mixture of 1 μmol/L Bodipy(493/503), 1 μmol/L Bodipy(558/568)-C12 or 5 μmol/L Bodipy(581/591)-C11, 0.2 μmol/L Mitotracker (Invitrogen), and 0.5 μg/mL Hochest (Beyotime) in serum-free culture medium for 20 min according to different purposes. Images were acquired using a confocal microscope (Olympus Corporation), an STED (Leica, Wetzlar, Germany), or an HIS-SIM (Computational Super-resolution Biotech, Guangzhou, China). Colocalization of Bodipy(558/568)-C12 and LDs/mitochondria was assessed *via* Manders' overlap coefficient using ImageJ 2.14.0 software.

2.5. Neomycin Texas-red conjugate

NTR was synthesized as previously described[26]. Briefly, Texas Red Succinimidyl Ester (TR, Invitrogen) was dissolved in *N*,*N*-dimethylformamide to make a 2.5 mmol/L Texas Red solution, after which neomycin sulfate was dissolved in 125 mmol/L K_2CO_3 solution to a final concentration of 2.5 mmol/L. Neomycin and TR were mixed at a molar ratio of 330:1 to make sure one TR per neomycin molecule, and the mixture was incubated at 4 °C for 3 days before being stored at −20 °C.

2.6. Tissue culture and treatment

FVB mice were decapitated at P2 and cleaned with 75% alcohol. Isolated the inner ears and transferred them to pre-cooled sterile HBSS. Then micro-dissected cochleae under a microscope to remove capsules and modiolus. The sensory epitheliums were separated from ligaments and seeded on Cell-tak (Corning) coated coverslips to be cultured in DMEM-F12 medium supplemented with 1% N_2 supplement (Gibco, Grand Island, NE, USA), 2% B27 solution (Gibco), and 50 μg/mL ampicillin (Sigma−Aldrich) in an incubator for 12 h to adapt. After that, cochlear explants from the treatment group were exposed to 0.5 mmol/L neomycin or NTR for 6 h followed by another 12 h recovery phase after drug withdrawal. Removed the culture medium and fixed the samples with 4% PFA in PBS for further immunostaining.

2.7. Cell culture and treatment

The House Ear Institute-Organ of Corti 1 cells (HEI-OC1) were cultured in DMEM (Gibco) supplemented with 10% FBS at 37 °C in a humidified incubator with 5% CO_2 and treated with a specific concentration of neomycin for different experimental purposes. The mouse proximal renal tubular cell line (TCMK-1) was purchased from American Type Culture Collection (Rockville, MD, USA). TCMK-1 cells were cultured in EMEM (Gibco) supplemented with 10% FBS at 37 °C in an incubator with 5% CO_2 and

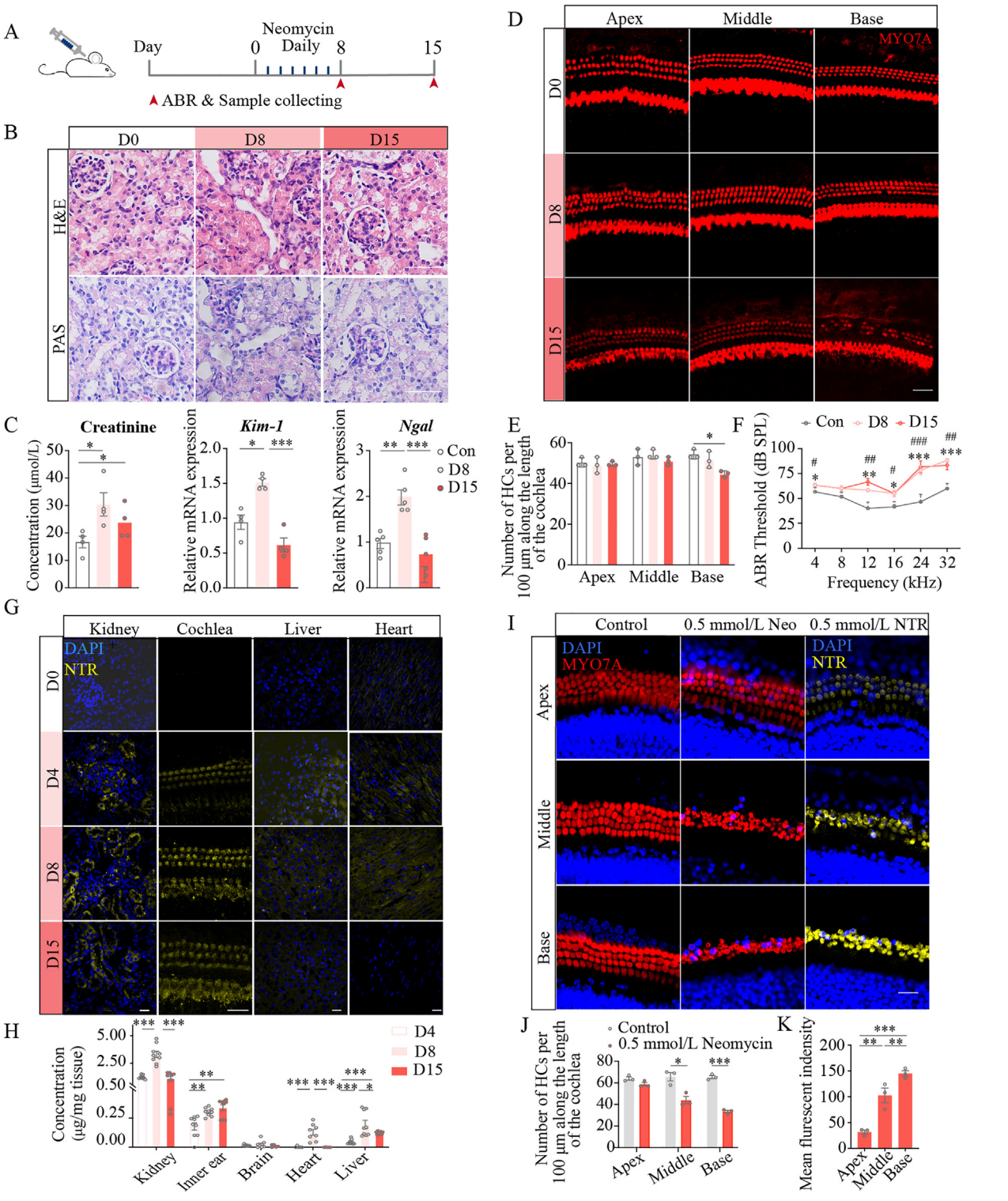

Figure 1 The characteristics of neomycin distribution in the cochlea and kidney correlate with ototoxicity and nephrotoxicity. (A) Schematic diagram of 200 mg/kg neomycin administration for 7 days followed by 7 days drug withdrawal in mice. (B) Histological photomicrographs of kidney tissue sections stained with H&E, PAS. Scale bar = 50 μm. (C) Analysis of serum creatinine, *Ngal* and *Kim*-1 mRNA levels ($n = 4-6$). (D) Representative confocal images of hair cells. Scale bar = 20 μm. (E) Quantification of MYO7A$^+$ hair cells of three turns of cochleae ($n = 3$). (F) ABR measurement of mice ($n = 3$). $^*P < 0.05$, $^{**}P < 0.01$, $^{***}P < 0.001$ D8 *vs*. control group. $^{\#}P < 0.05$, $^{\#\#}P < 0.01$, $^{\#\#\#}P < 0.001$ D14 *vs*. control group. (G) Representative confocal images depicting NTR accumulation in various organs of mice. Scale bar = 20 μm. (H) Determination of drug concentration in various tissues detected by HPLC−MS/MS ($n = 9$). Con: mice treated with saline once daily for 7 days; D4: mice treated with 200 mg/kg neomycin once daily subcutaneously for 3 days; D8: mice treated with 200 mg/kg neomycin once daily subcutaneously for 7 days; D15: mice treated with 200 mg/kg neomycin once daily subcutaneously for 7 days followed by drug withdrawal for 7 days. (I)

treated with a specific concentration of neomycin for different experimental purposes.

2.8. siRNA transfection

HEI-OC1 and TCMK-1 cells were transfected with 50 nmol/L siRNA targeting mouse *Pgc-1α* or 50 nmol/L control siRNA (Genepharma, Shanghai, China) using Lipofectamine reagent (Invitrogen) when the cells were around 40% confluent. Cells were transfected for 48 h for further processing. The siRNA sequences targeting *Pgc-1α* were as follows: siRNA 5′-GUAGCGACCAAUCGGAAAUTT-3′ and 5′-AUUUCCGAUUGGUCGCUACTT-3′.

2.9. Real-time PCR and Western blotting

Total RNA was isolated from tissues and cells using TRIzol method according to the manufacturer's instructions and quantified *via* ultraviolet spectrophotometry. Complementary DNA was synthesized using the RT reagent (Vazyme, Nanjing, China). SYBR qPCR mastermix (Vazyme) was subsequently used to amplify cDNA in a CFX96 real-time PCR detection system (Bio-Rad, Hercules, CA, USA). The $2^{-\Delta\Delta CT}$ method was used to analyze the relative fold changes. The primer sets used are described in Supporting Information Table S1.

Cells and tissues were lysed with cold RIPA Lysis Buffer plus PMSF (Beyotime) for 30 min at 4 °C. Protein concentration was determined by BCA Protein Assay Kit (Beyotime) after centrifuging the lysates at 12,000×*g* for 10 min at 4 °C. A total of 30 μg of each kidney protein sample or 15 μg of each cell sample and explant sample were separated *via* SDS-PAGE and subsequently transferred to polyvinylidene fluoride membranes (Millipore, Bedford, USA). After blocking with 5% BSA for 1 h at RT, the membranes were incubated with anti-PLIN1-3,5 (1:1000, Proteintech Group, Rosemont, IL, USA), anti-PLIN4 (1:1000, Novus, Littleton, CO, USA) or anti-*β*-actin antibodies (Cell Signaling Technology, Danvers, MA, USA) at 4 °C overnight. After washing with TBST, the membranes were incubated with horseradish peroxidase-linked anti-mouse or anti-rabbit secondary antibodies (Cell Signaling Technology) at 37 °C for 1 h. The signals were detected with an enhanced chemiluminescence kit (Bio-Rad) and the signal were visualized with a ChemiDoc XRS + system (Bio-Rad). The protein band density was calculated by ImageJ 2.14.0 software and normalized to *β*-actin.

2.10. Single-nuclear RNA-Seq

Three FVB mice were sacrificed at P20. Cochleae and kidneys collected from different mice were combined as a single sample, respectively. After homogenizing and centrifuging, the nuclei were partitioned into individual droplets with a barcode gel bead using the 10X chromium instrument (10X Genomics, Pleasanton, CA, USA). The R packages Seurat v.4.3.1, ggplot2 v.3.4.2, and dplyr v.1.1.2 were used to process data analysis. Data were normalized and scaled using SCTransform. ElbowPlot was used to determine the number of useful principal components. Principle analysis dimensions were reduced using UMAP. Marker genes were identified using FindAllMarkers in Seurat.

2.11. Lipidomics

For sample collection, P15 mice were decapitated and otic capsules were isolated from both sides. Both sides of inner ear from a single mouse were combined into one sample, and 20 mg of renal tissue was weighed as one kidney sample. LPE 14:0 (Avanti Polar Lipids, Alabaster, AL, USA) was used as an internal standard. Samples were homogenized in 75% methanol with 10 μg/mL LPE 14:0 (Avanti Polar Lipids) at 4 °C, mixed with 500 μL of methyl tertiary butyl ether per sample at RT for 1 h. Then 125 μL of water was added per sample, followed by centrifugation at 14,000 rpm in the centrifuge (5804R, Eppendorf, Hamburg, Germany) at RT for 15 min. 300 μL of supernatant was concentrated by nitrogen concentrators and redissolved in a working solution (acetonitrile:isopropanol: water = 60:35:5, *v*/*v*/*v*), and then detected by a 5500 triple-quad mass spectrometer (AB SCIEX, Los Angeles, CA, USA) equipped with an ESI source coupled to a Shimadzu Prominence UHPLC system (Shimadzu, Kyoto, Japan) in both positive and negative polarities. For chromatographic separation, a Thermo Hypersil GOLD HPLC column was heated to 55 °C. The mobile phase of the liquid system was consisted of solvent A (acetonitrile:water = 40:60, *v*/*v*, containing 5 mmol/L ammonium formate and 0.1% formic acid) and solvent B (isopropanol:acetonitrile = 90:10, *v*/*v*, containing 5 mmol/L ammonium formate and 0.1% formic acid). The gradient elution procedure was set as follows: 0−2 min (20% B), 2−8 min (20%−60% B), 8−23 min (60%−80% B), 23−23.1 min (80%−95% B), 23.1−25 min (95%−20% B), and 25−30 min (20% B). For lipid analysis, the ESI source conditions were set as follows: IonSpray Voltage, 4500 V or −4500 V; Ion Source Gas 1 and Ion Source Gas 2, 50 psi; Curtain Gas, 35 psi; Collision Gas, 10 psi; and Temperature, 500 °C. TOF MS scan in positive model, *m*/*z* 300.2−972.8 Da; Collision Energy, 10−50 V; TOF MS scan in negative model, *m*/*z* 255.1−939.6 Da; Collision Energy, −60 to −10 V. Data were analyzed by Analyst TF 1.7, MultiQuant 3.0 software (AB SCIEX) and R ("EnhancedVolcano", "ComplexHeatmap" packages). Differences between the control and neomycin treatment groups were determined by statistical analysis. Principal component analysis (PCA) was implemented using MetaboAnalyst (http://www.metaboanalyst.ca/).

2.12. Drug concentration detection

10 mg of heat, kidney, liver, or brain tissue was homogenized in 1.2 mL of distilled water on ice for further processing. 2 inner ears were combined as a single sample after removing Otic capsules and then homogenized in 0.3 mL of distilled water by an electric homogenizer for further sample processing. HEI-OC1 and TCMK-1 cells were cultured in 10 mm petri dishes and treated with 2 mmol/L neomycin for 24 h. Commercial assay kits (Keygentec, Nanjing, China) were used to isolate the cytoplasm,

Representative confocal images of three turns of the cochlear explants. Scale bar = 20 μm. (J) Quantification of $MYO7A^+$ hair cells of the cochlear explants ($n = 3$). (K) Quantification of fluorescence area of NTR in cochlear explants ($n = 3$). Con, cochlear explants cultured with culture media for 18 h; Neo, cochlear explants treated with 0.5 mmol/L neomycin for 6 h followed by 12 h recovery. *Ngal*, neutrophil gelatinase-associated lipocalin; *Kim-1*, kidney injury molecule 1. The results are presented as the means ± SEM. $^*P < 0.05$, $^{**}P < 0.01$, $^{***}P < 0.001$.

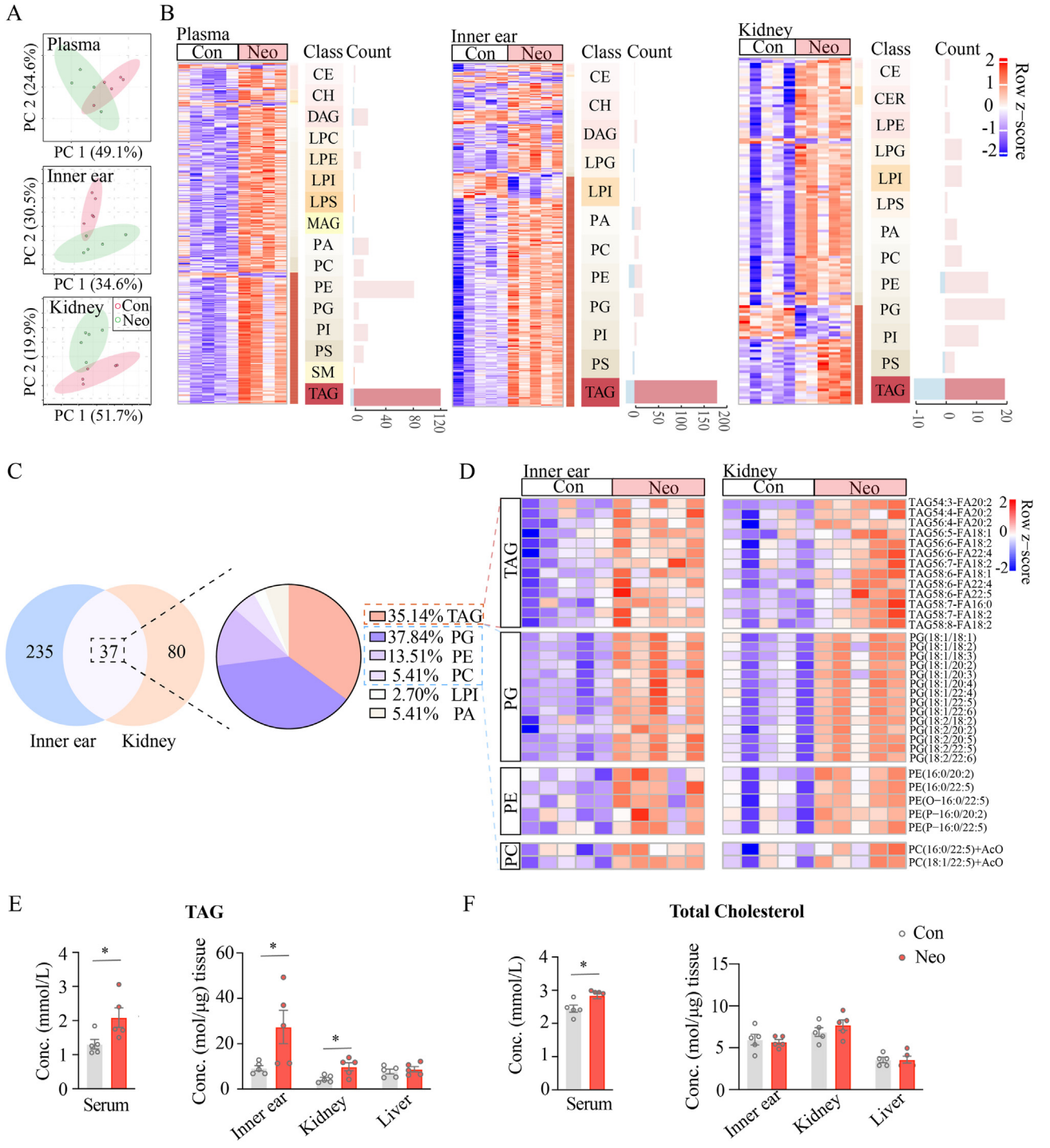

Figure 2 Lipid metabolism disorder and TAG accumulation in neomycin-induced renal injury and hearing impairment. (A) PCA score plot of lipidomics in plasma, inner ears, and kidneys with or without neomycin treatment. (B) Heatmaps and counts illustrating significantly changed lipids ($P < 0.05$) in plasma, inner ears, and kidneys. (C) Venn plot depicting common significantly elevated lipids between inner ears and kidneys, accompanied by a pie chart categorizing the 37 significantly changed lipids. (D) Heatmaps illustrating common changed species of TAG, PG, PE, and PC in the inner ears and kidneys. (E) Quantitative assessment of TAG levels. (F) Quantitative assessment of total cholesterol levels. Con: mice treated with saline once daily for 7 days; Neo: mice treated with 200 mg/kg neomycin once daily for 7 days. The results are presented as the means ± SEM. $^*P < 0.05$. $n = 5$.

mitochondria, and nuclei according to the manufacturer's instructions. The quantification of neomycin in the samples was performed using HPLC−MS/MS as previously described[27]. Samples with amikacin as an internal standard were treated with extraction solution (10 mmol/L ammonium acetate, 0.4 mmol/L EDTA, 0.5% NaCl, and 2% TCA) to release neomycin from proteins. The samples were vortexed at 2000 rpm in the centrifuge (5804R, Eppendorf) for 10 min, left on ice for 30 min, and then

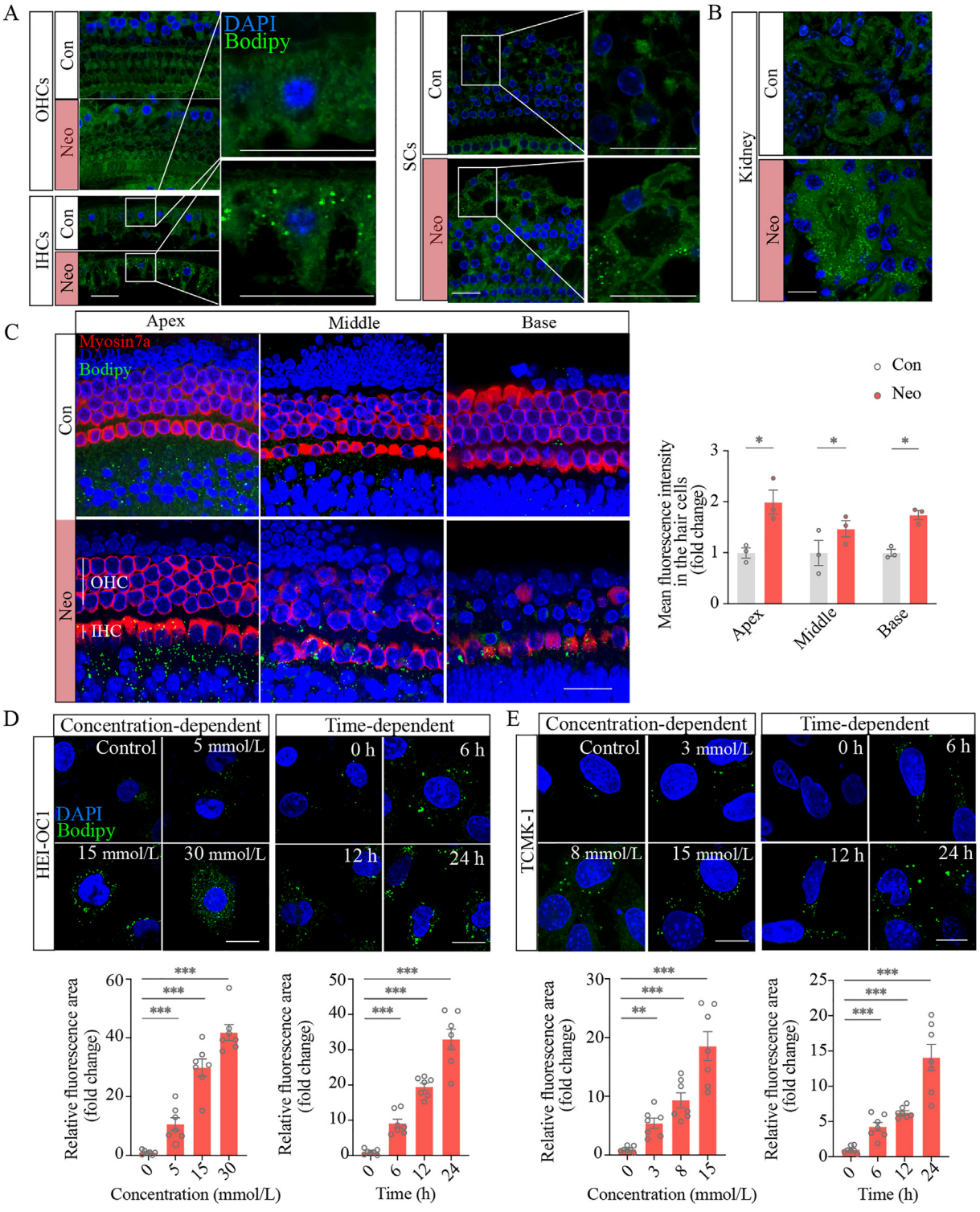

Figure 3 Characteristics of LD accumulation induced by neomycin in the cochlea and kidney. (A) Representative confocal images of Bodipy (493/503) staining detecting LDs in the inner hair cells, outer hair cells, and supporting cells of cochleae, respectively. Con: mice treated with saline once daily for 7 days; Neo: mice treated with 200 mg/kg neomycin once daily for 7 days. (B) Representative confocal images of Bodipy (493/503) staining detecting LDs in kidneys. (C) Representative confocal images of Bodipy (493/503) staining depicting LDs in cochlear explants, alone with quantification of LDs fluorescence in hair cells ($n = 3$). Con, cochlear explants cultured with culture media for 18 h; Neo, cochlear explants treated with 0.5 mmol/L neomycin for 6 h followed by 12 h recovery. (D, E) Representative confocal images of Bodipy (493/503) staining illustrating LDs in HEI-OC1 and TCMK-1 cells treated with varying neomycin concentrations. Over different durations, along with quantification of fluorescence area of LDs ($n = 7$). The results are presented as the means ± SEM. $^{*}P < 0.05$, $^{**}P < 0.01$, $^{***}P < 0.001$. Scale bar = 20 μm.

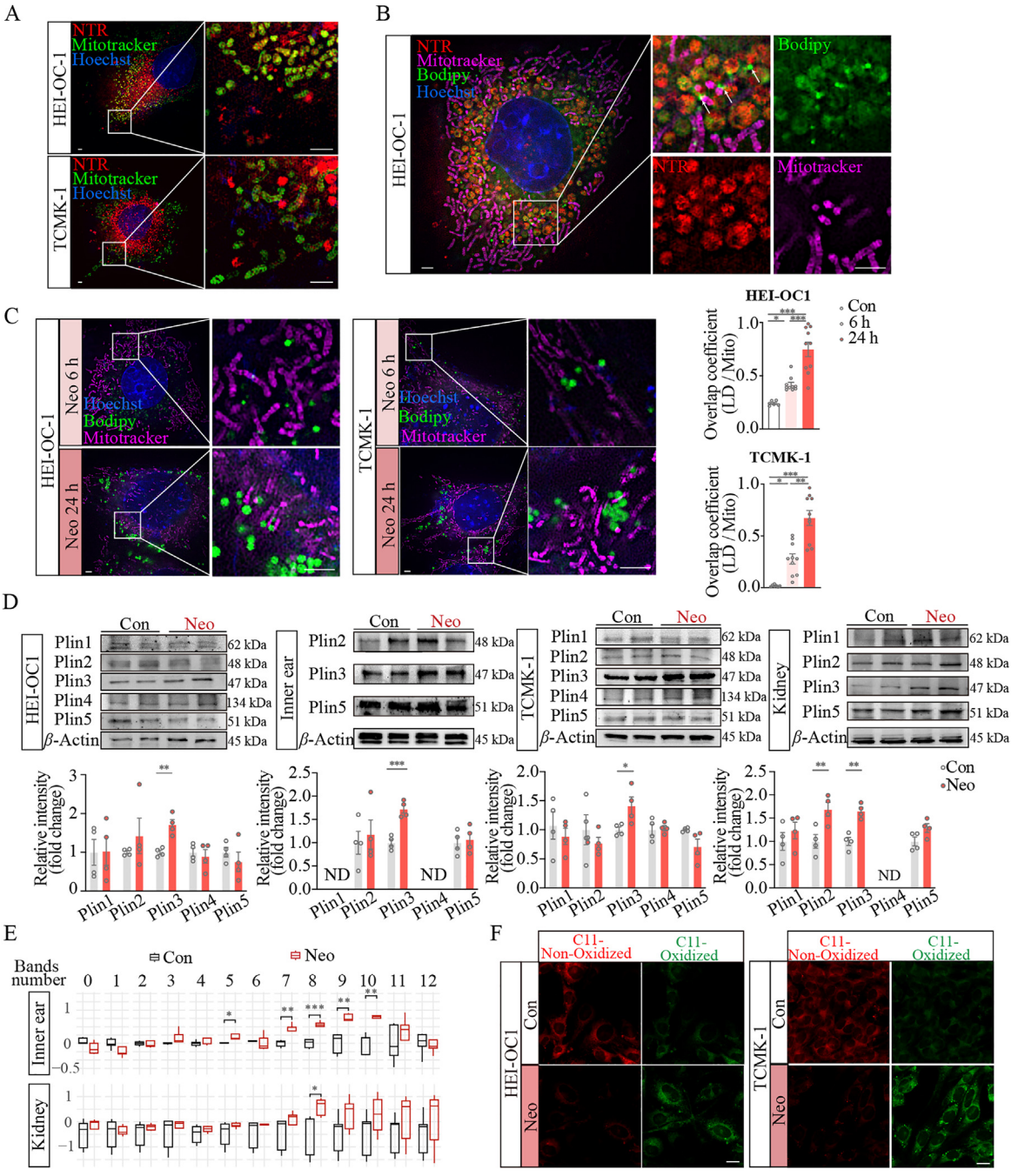

Figure 4 Neomycin targeted mitochondria and accelerated the interactions between mitochondria and LDs. (A) Representative HIS-SIM images of NTR, and Mitotracker deepred illustrating neomycin and mitochondria in HEI-OC1 and TCMK-1 cells after 2 mmol/L NTR treatment for 24 h. Scale bar = 2 μm. (B) Representative HIS-SIM images of NTR, Bodipy(493/503), and Mitotracker deepred illustrating neomycin, LDs, mitochondria, and the interactions among them (white arrow) in HEI-OC1 cells after NTR treatment for 24 h. Scale bar = 2 μm. (C) Representative confocal images of Mitotracker deepred and Bodipy(493/503) co-staining illustrating the interactions between mitochondria and LDs in HEI-OC1 and TCMK-1 cells, respectively. Relative cellular co-localization of Bodipy(493/503) and Mitotracker deepred was quantified by overlap coefficients (n = 15−20). Scale bar = 2 μm. (D) Representative images of PLIN family protein expression in HEI-OC1, TCMK-1 cells, kidneys, and inner ears (n = 4). (E) Relative quantitative analysis of the relative abundance for TAGs and PLs containing double bonds by LC−MS (n = 5). Con, mice treated with saline aqueous solution for 7 consecutive days; Neo, mice treated with 200 mg/kg neomycin for 7 consecutive days. (F) Representative confocal images of Bodipy(581/591)-C11 staining detecting lipid ROS in HEI-OC1 and TCMK-1 cells. Scale bar = 20 μm. Con, cells cultured in blank culture media for 6 or 24 h; Neo, HEI-OC1 cells treated with 2 mmol/L NTR or 15 mmol/L or TCMK-1 cells treated with 2 mmol/L NTR or 8 mmol/L neomycin for 6 or 24 h. ND, not detected. The results are presented as the means ± SEM. *P < 0.05, **P < 0.01, ***P < 0.001.

centrifuged at 3000 rpm in the centrifuge (5804R, Eppendorf) at RT for 10 min. Afterwards, the supernatant was transferred to new tubes and adjusted to pH 6.5 with 20% NaOH or 1 mol/L HCl, and loaded into an Accell Plus CM SPE cartridge, followed by elution with 2.3% ammonia in water. Then, the eluate was then concentrated by nitrogen concentrators and redissolved in distilled water, followed by centrifugation at 18,000 × *g* for 5 min. 10 μL of supernatant was detected by an LC−MS/MS system consisting of a Shimadzu HPLC system 20A and an AB API4000 quadrupole mass spectrometer with an electrospray ionization interface. A SIELC Obelisc R column (2.1 mm × 150 mm, 5 μm) was used to separate the neomycin. The mobile phase of the liquid system consisted of solvent A (1% formic acid in deionized water and 10 mmol/L ammonium formate) and solvent B (acetonitrile). The gradient elution procedure was set as follows: 0−3 min (85% B), 3−4 min (85%−5% B), 4−10 min (5% B), 10−11 min (5%−85% B), 11−15 min (85% B). Multiple-reaction monitoring was used to monitor the analyte and internal standard. The selected mass transitions were *m/z* 586.6 → 425.5 for IS, *m/z* 455.3 → 163.1 for NEO. Collison Gas, 12 Arb; Curtain Gas, 30 Arb; Ion Source Gas 1, 45 Arb; and Ion Source Gas 2, 65 Arb; Declustering Gas, 120 V; Collision Energy, 52 V; Temperature, 450 °C. Data acquisition and analysis were performed using Analyst TF 1.5.1 software (SCIEX). The values were normalized to the protein content or tissue weight in each sample, which were determined by a BCA protein assay.

2.13. Hair cell counts

For HC quantification, cochleae were imaged with a 40 × objective, and the remaining MYO7A$^+$ HCs were counted. For live cells, cell viability was examined with a cell counting kit-8 (Beyotime) according to the manufacturer's instructions. Cells were seeded in 96 well plates and treated with neomycin for a specified period. Then the CCK-8 reagent was added to cells followed by incubation for 1 h. Cell viability was determined using a microplate reader (Bio-tek instruments, Winooski, VT, USA) at 450 nm.

2.14. Seahorse mitochondrial stress test

Cell metabolic/bioenergetic profiles were evaluated with an XF Cell Mito Stress Assay in a Seahorse XFe24 analyzer (Seahorse Bioscience, MA, USA). HEI-OC1 and TCMK-1 cells were plated in 96-well SeahorseXF cell culture plates at a density of 5000 cells/well, after which the cells were treated with neomycin. Seahorse XF calibration solution was added to utility plates at the same time. The test plates were placed on the utility plate at 37 °C without CO_2 to hydrate the probe overnight in the incubator. The day before the experiment on the machine, the Seahorse XF Base Medium was heated to 37 °C, the pH was adjusted to 7.4 with NaOH, and the solution was filtered to prepare the detection solution. The solution was subsequently placed in a 37 °C water bath for later use. On the day of the experiment, the cells were observed under a microscope, the complete medium was replaced with detection solution and the cells were placed in a 37 °C CO_2-free incubator for 1 h. Additionally, 1 μmol/L oligomycin, 3 μmol/L FCCP, 1 μmol/L rotenone or 1 μmol/L antimycin A was added to the four dosing holes A, B, C, and D on the test plate, respectively. The experimental program was set up on the Seahorse instrument and computer, after which the test plate and the utility plate containing the calibration solution were placed on the instrument tray together. The utility plate was replaced with a test plate for detection after the probes were automatically calibrated by the instrument. After the detection was completed, Ware Software was used for data analysis.

2.15. Biochemical analysis

Commercial kits were used to measure the levels of serum creatinine, TG and total cholesterol in serum or tissue lysates (Elabscience, Wuhan, China) according to the manufacturer's instructions.

2.16. Histological analysis

For histological analysis, a portion of renal cortex was fixed with 4% PFA in PBS, embedded in paraffin wax, and then sliced into 5 μm sections for hematoxylin and eosin (H&E) staining and periodic acid-schiff (PAS) staining, and imaged by an upright microscope (Olympus Corporation).

2.17. Transmission electron microscopy scanning

For electron microscopy imaging, a part of renal cortex was fixed in 2.5% glutaraldehyde in cacodylate buffer solution (pH 7.4) overnight at RT. Then, the samples were post-fixed in 1% osmium tetroxide phosphate buffer solution, dehydrated, and embedded in epoxide resin. Thin sections were cut with an LKB Ultratome IV (LKB Instruments, Bromma, Sweden), stained with uranyl acetate and lead citrate, and imaged with a Hitachi 7500 electron microscope (Hitachi, Japan).

2.18. Cyrosectioning

A portion of kidney was fixed with 4% PFA in PBS at 4 °C overnight and dehydrated in 20% and 30% sucrose-phosphate-buffered saline solution successively at 4 °C until it sank to the bottom of the tube. The dehydrated tissues were embedded in O.C.T compound (Sakura Finetek, Torrance, CA, USA) and stored at −80 °C overnight. Frozen sections were then sliced into 10 μm sections using a cryostat (Leica CM 1850, Leica) for further immunostaining.

2.19. Statistical analysis

Statistical analyses were conducted using Graphpad Prism software (Graphpad9 software, La Jolla, CA, USA). Data are expressed as mean ± standard error of mean (SEM). To test for statistical significance, the Student's *t*-test was used to compare two different groups. Comparisons between more than two groups were analyzed using two-way analysis of variance (ANOVA) with Dunnett's test, or one-way ANOVA with Tukey's test. $P < 0.05$ was considered to indicate statistical significance.

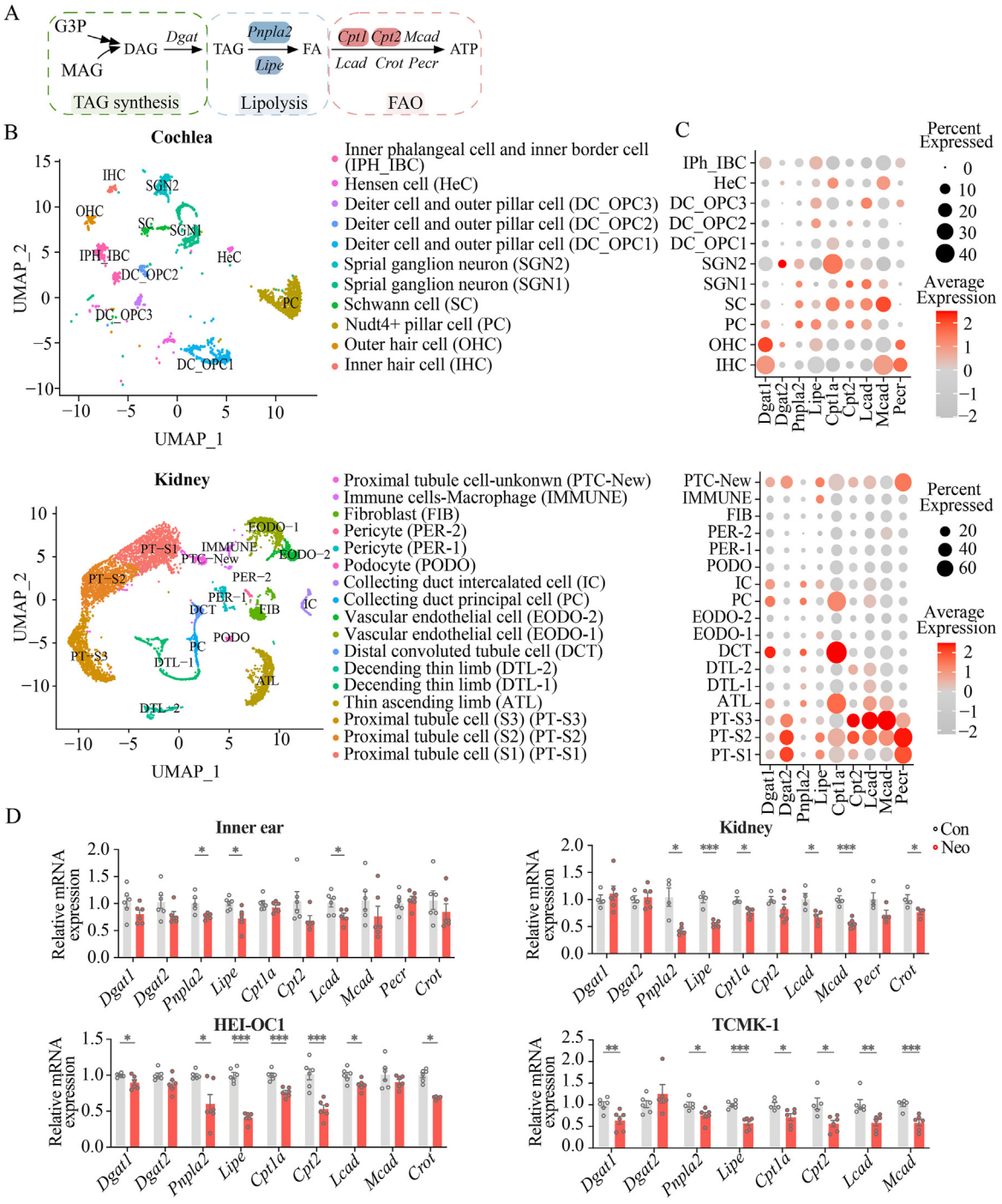

Figure 5 Single cell sequencing analysis and neomycin downregulated the genes related to lipolysis and FAO. (A) Schematic depiction of primary genes involved in TAG synthesis, lipolysis and FAO. (B) UMAP visualization of cells in mouse cochlea and kidney. (C) Dot plot illustrating the relative expression of genes involved in TAG metabolism among clusters in kidneys and cochleae. (D) Relative mRNA expression of genes related to TAG synthesis, lipolysis and FAO in the inner ears, kidneys, HEI-OC1 and TCMK-1 cells (n = 5−6). Experiment groups: Con, cells cultured in blank culture media for 24 h; Neo, HEI-OC1 cells treated with 15 mmol/L or TCMK-1 cells treated with 8 mmol/L neomycin for 24 h. Con, mice treated with saline aqueous solution for 7 consecutive days; Neo, mice treated with 200 mg/kg neomycin once daily subcutaneously for 7 consecutive days. G3p, glycerol-3-phosphate; MAG, monoacylglycerol; DAG, diacylglycerol; TAG, triacylglycerol; FA, fatty acid; *Dgat1*, diacylglycerol *O*-acyltransferase 1; *Dgat2*, diacylglycerol *O*-acyltransferase 2; *Pnpla2*, patatin-like phospholipase domain containing 2; *Lipe*, hormone-sensitive lipase; *Cpt1a*, carnitine palmitoyltransferase 1A; *Cpt2*, carnitine palmitoyltransferase 2; *Lcad*, long-chain acyl-CoA dehydrogenase; *Mcad*, medium-chain acyl-CoA dehydrogenase; *Crot*, carnitine *O*-octanoyltransferase; *Pecr*, peroxisomal *trans*-2-enoyl-CoA reductase. The results are presented as the means ± SEM. *$P < 0.05$, **$P < 0.01$, ***$P < 0.001$.

3. Results

3.1. *Spatiotemporal characteristics of neomycin distribution in the cochlea and kidney correlate to its specific ototoxicity and nephrotoxicity*

To investigate the link between neomycin-induced toxicity and drug accumulation, postnatal Day 8 mice were administrated with 200 mg/kg neomycin subcutaneously daily for 7 days, followed by a 7-day of drug withdrawal (Fig. 1A). H&E and PAS staining revealed kidney tubular injury characterized by brush border disruption and tubular dilation after a 7-day treatment with neomycin, which subsequently self-restored on Day 15 (Fig. 1B). Additionally, the levels of serum creatinine, as well as specific acute kidney injury markers—the gene expression of neutrophil gelatinase-associated lipocalin (*Ngal*) and kidney injury molecule-1 (*Kim-1*)—were significantly increased on Day 8 and subsequently decreased to the normal levels on Day 15 compared to Day 8 (Fig. 1C). For ototoxicity assessment, no significant loss of hair cells in any of the three turns of the cochleae was observed on Day 8, but hair cell loss in the basal turn occurred on Day 15 (Fig. 1D and E), indicating a progressive injury of the hair cells. In contrast, the impairment of hearing function occurred before the noticeable loss of hair cells, as evidenced by the threshold elevation in the auditory brainstem response (ABR) across almost all frequencies, particularly at higher frequencies such as 24 and 32 kHz on both Day 8 and Day 15 (Fig. 1F). Ciliary derangement of hair cells also occurred on Day 8 and was aggravated on Day15 (Supporting Information Fig. S1A). No obvious changes in histopathology were observed in the livers or hearts after drug administration (Fig. S1B).

To visualize the spatial distribution of neomycin in kidneys, ears and other tissues, mice were treated with NTR for 7 days followed by drug withdrawal for 7 days. NTR predominantly accumulated in renal proximal tubular cells and hair cells after consecutive NTR administration. Noticeable retention of the drug was observed in hair cells even after drug withdrawal for 7 days, while NTR in renal proximal tubular cells was eliminated on Day 15 (Fig. 1G). These findings were consistent with the recovery of renal function and the exacerbation of hearing function after drug withdrawal. In contrast, there was no significant accumulation of NTR in the livers or hearts. Quantification of the neomycin distribution by HPLC−MS/MS confirmed the characteristics of neomycin distribution in different organs (Fig. 1H). When cochlear explants were exposed to 0.5 mmol/L NTR, NTR had the highest distribution in basal hair cells, followed by the middle turns and apex turns. Fluorescein TR, which was not conjugated with neomycin, did not enter hair cells, demonstrating the selective toxicity of NTR towards hair cells as neomycin (Fig. S1C). Consistently, the damage and absence of basal hair cells were most evident among the three turns (Fig. 1I−K), reflecting the more pronounced damage in ABR changes at the higher frequencies.

3.2. *Lipid metabolism disorders and triacylglycerol accumulation are induced by neomycin in the inner ear and kidney*

Our previous study found that AGs preferentially targeted mitochondria and subsequently induced changes in mitochondrial structure and function, along with the deposition of LDs[10]. Here, we explored alterations in lipid profiles associated with neomycin-induced renal injury and hearing loss. Targeted lipidomics by UHPLC/ESI-QTOF-MS analysis identified 22 lipid classes in plasma, kidney, and inner ear samples (Supporting Information Table S2). PCA score plots depicted distinct clustering and separation of lipidomic profiles between the control and neomycin-treated groups, indicating a discernible difference in lipidomic data between the two groups (Fig. 2A). Further analysis revealed that 335 of 1091 species from 16 classes exhibited statistically significant changes in plasma concentration; 320 of 1150 species from 12 classes exhibited statistically significant changes in the inner ear; and 133 of 1149 species from 13 classes exhibited statistically significant changes in the kidney (Fig. 2B). Volcano plot analysis revealed that the number and intensity of changes in TAGs after neomycin administration were significantly greater than those of other types of lipids, with over 180 types of TAGs elevated in the inner ears (Supporting Information Fig. S2). Among the elevated lipids, 37 species were commonly changed in both the kidneys and inner ears. Thirteen of them belong to TAG (35.14%), 14 of them belong to phosphatidylglycerol (PG), 5 belong to phosphatidylethanolamine (PE), 2 belong to phosphatidylcholine (PC), 2 belong to phosphatidic acid (PA), and 1 belongs to lysophosphatidylinositol (LPI) (Fig. 2C and D). Then, quantitative analysis further showed that TAG levels increased to 1.6, 2.9, and 2.0 times those of the control groups in plasma, inner ears, and kidneys after neomycin treatment, respectively (Fig. 2E). However, there were no significant changes in liver TAG levels between the two groups. Concurrently, no significant differences in total cholesterol levels were observed between the control group and the neomycin treatment group in the kidneys, inner ears, or livers (Fig. 2F).

3.3. *Lipid droplets accumulate in cochlear hair cells and renal tubular cells after neomycin treatment*

TAGs are known as the core component of LDs, and the phospholipids PG, PE and PC play crucial roles in the membranes of organelles. Recently, an increasing number of studies have demonstrated that LDs are highly dynamic organelles and are involved in the occurrence and development of various diseases[28]. However, there are few published studies concerning the role of LDs in drug-induced ototoxicity and nephrotoxicity. Bodipy (493/503) staining demonstrated that, compared with that in the control group, LD accumulation increased in the cochleae of mice treated with neomycin for 7 days, particularly in the inner hair cells and supporting cells (Fig. 3A). Similarly, compared with those in the control group, increased LD accumulation was also observed in the kidneys of mice after neomycin treatment for 7 days (Fig. 3B). However, there was no LD deposition in the livers of mice treated with neomycin (Supporting Information Fig. S3A). In cochlear explants, some physiological LDs can be observed in all three turns of supportive cells. Neomycin treatment induced LD accumulation in cochlear explants, especially in inner hair cells and supportive cells (Fig. 3C). *In vitro*, HEI-OC1 (a commonly used auditory cell line) and TCMK-1 (a kidney tubular epithelial cell line) cells were treated with various concentrations of neomycin for different durations. Both cell lines exhibited significant uptake of neomycin at 3 h, after which the uptake progressively increased over time (Fig. S3B). Quantitative analysis of confocal images illustrated that LD accumulation increased in both a time-dependent and concentration-dependent manner in the two cell lines (Fig. 3D and E).

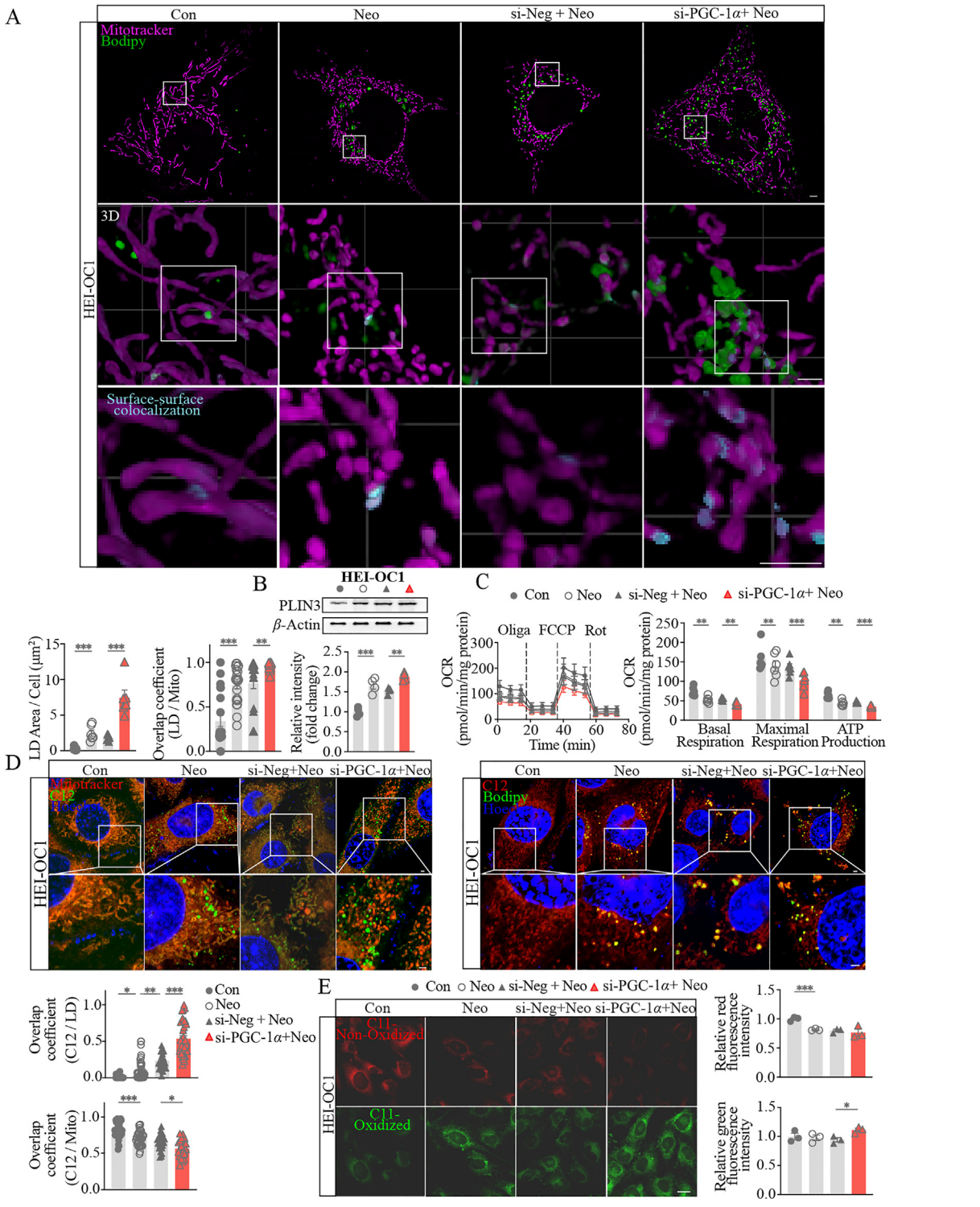

Figure 6 *Pgc-1α*$^{-/-}$ aggravated neomycin-induced lipid metabolism disorder and lipid oxidation *in vitro*. (A) Representative HIS-SIM images depicting Bodipy(493/503), and MitoTracker Deep Red depicting LDs, mitochondria in HEI-OC1 cells after NTR treatment for 24 h, and quantification of fluorescence area as well as numbers of LDs (n = 15−20). Scale bar = 2 mm. (B) Representative images of PLIN 3 protein expression in HEI-OC1 cells (n = 4). (C) Fundamental mitochondrial function detection in HEI-OC1 cells (n = 4). (D) Representative confocal images of Bodipy(558/568)-C12, Bodipy(493/503) and Mitotracker DeepRed staining monitoring FAs deposition in HEI-OC1 cells. Relative cellular co-localization between C12 and Mitotracker deep red, C12 and Bodipy(493/503) were quantified by overlap coefficients (n = 15−20). Scale bar = 2 μm. (E) Representative confocal images of Bodipy(581/591)-C11 staining detecting lipid ROS in HEI-OC1 cells (n = 4). Scale bar = 20 μm. Experiment groups: Con, cells cultured in blank culture media for 24 h; Neo, cells treated with 15 mmol/L neomycin for 24 h; Neg-siRNA + Neo, cells treated with 15 mmol/L neomycin after cultured with negative siRNA mixture for 48 h; PGC-1α-siRNA + Neo, cells treated with 15 mmol/L neomycin after cultured with PGC-1α siRNA mixture for 48 h. The results are presented as the means ± SEM. *P < 0.05, **P < 0.01, ***P < 0.001.

3.4. *Neomycin targets mitochondria and exacerbates the pathological interactions between droplets and mitochondria*

To clarify the positional relationships among the intracellular NTR distribution, LDs, and mitochondria, high sensitivity structured illumination microscopy (HIS-SIM) was used, and it was found that some NTR colocalized with mitochondria, and some distributed around mitochondria in a lipid droplet-like morphology (Fig. 4A). Some direct contacts (white arrows) among the NTR (red), LDs (green) and mitochondria (pink) regions were observed (Fig. 4B). The contacts between LDs and mitochondria significantly increased over time with increasing LD size (Fig. 4C). Quantitative analysis of neomycin distribution in separated subcellular organelles by HPLC−MS/MS revealed that neomycin was predominantly distributed in mitochondria rather than in the cytoplasm and nucleus (Supporting Information Fig. S4A). Perilipin (PLIN) family, specific coating proteins around LDs, has been reported to play a crucial role in LD formation and the connection between LDs and mitochondria[29]. Here, we investigated whether the Perilipin family participates in the toxicity induced by neomycin. Western blotting revealed an increase in PLIN 3 expression in both tissues and cell lines after neomycin treatment, implying the potential involvement of PLIN3 in the interactions between mitochondria and LDs (Fig. 4D).

Our further lipomic analysis found that neomycin caused a notable increase in lipids containing multiple unsaturated bonds in the inner ears and kidneys. The levels of unsaturated lipids containing 5, 7, 8, 9, or 10 double bonds increased significantly in the inner ear, and unsaturated lipids containing fatty acids with 8 double bonds increased significantly in the kidney after 7 days neomycin exposure (Fig. 4E). It is well-known that the more double bonds unsaturated lipids contain, the more vulnerable organelle membranes are to oxidative stress[30]. Consistently, the oxidized-C11 (green) was present mainly in the neomycin group and exhibited a lipid droplet-like morphology, indicating that neomycin triggered lipid peroxidation in both two cell lines (Fig. 4F). The MitoSOX probe also showed that mitochondrial ROS were elevated in neomycin-treated OC-1 and TCMK-1 cells (Fig. S4B).

3.5. *Neomycin downregulates the expression of genes governing lipolysis and fatty acid oxidation in the inner ear and kidney*

To determine the influence of neomycin on lipid metabolism pathways, the expression of genes involved in TAG synthesis, lipolysis, and FAO was examined (Fig. 5A). Single-nuclear RNA-sequencing was used to determine the relative expression of genes involved in the TAG metabolism pathway. A total of 1977 cells collected from the cochlear sample were divided into 11 clusters, and 8780 cells collected from the kidney sample were divided into 17 clusters (Fig. 5B, Supporting Information Fig. S5). A dot plot demonstrated that genes related to TAG synthesis, lipolysis and FAO were predominantly expressed in cochlear hair cells and renal proximal tubular cells, indicating more vigorous TAG synthesis and FAO in these two cell types than in the other cell types (Fig. 5C). TAG synthesis-related genes, namely *Dgat1*, and the FAO-related genes *Mcad* and *Pecr* exhibited relatively high expression in hair cells. *Dgat2*, *Cpt1a*, *Cpt2*, *Lcad*, *Mcad and Pecr* were abundantly expressed in renal proximal tubular cells. Q-PCR analysis revealed that neomycin mainly downregulated the genes related to lipolysis (*Pnpla2* and *Lipe*) and FAO without significantly influencing the TAG synthesis gene *Dgat1/2* in the inner ears and kidneys of neomycin-treated mice (Fig. 5D).

3.6. *Pgc-1α$^{-/-}$ exacerbates neomycin-induced lipid droplet−mitochondria interactions and imbalances in lipid homeostasis in vitro*

Our previous study revealed that AGs significantly decreased the expression of PGC-1α, a key regulator of mitochondrial function and energy metabolism, in the inner ears and kidneys[10]. Consistently, the present study also demonstrated that PGC-1α was downregulated at both the mRNA and protein levels after neomycin treatment (Supporting Information Fig. S6A). *Pgc-1α* was silenced in two cell lines to further explore the LD−mitochondrion interactions in neomycin-induced ototoxicity and nephrotoxicity. The efficiency of *Pgc-1α* gene silencing in HEI-OC1 and TCMK-1 cells were 75% and 73%, respectively. No significant difference in cell viability was observed after *Pgc-1α* gene silencing in HEI-OC1 or TCMK-1 cells (Fig. S6B). Cell viability decreased in the *Pgc-1α* silenced group after neomycin treatment compared with the negative silence group, indicating that *Pgc-1α* silencing promoted neomycin-induced cell damage (Fig. S6C). Bodipy (493/503) staining demonstrated that *Pgc-1α* silencing in HEI-OC1 and TCMK-1 cells increased the accumulation of LDs as well as the interactions between mitochondria and LDs after neomycin treatment (Fig. 6A, Fig. Supporting Information Fig. S7A). Meanwhile, *Pgc-1α* silencing also enhanced the neomycin-induced expression of LD-coated protein PLIN3 (Fig. 6B, Fig. S7B). Furthermore, mitochondrial function was assessed through the oxygen consumption rate *via* a Seahorse energy metabolism analyzer. Compared with those in negative control group, basal respiration, maximal respiration, and capability of ATP production decreased in the *Pgc-1α* silenced group after neomycin treatment, indicating more severe mitochondrial damage (Fig. 6C, Fig. S7C).

Intracellular lipid homeostasis mainly depends on the dynamic relationship between LD synthesis and turnover. FAs can be stored as TAGs in LDs, which can in turn release and transfer free FAs into mitochondria for energy production. To explore the impact of *Pgc-1α* deficiency on intracellular lipid homeostasis after neomycin treatment, Bodipy(558/568)-C12 was used to track lipid trafficking with LDs (Bodipy 493/503) or mitochondria (MitoTracker Deep Red) in two cell lines (Fig. 6D, Fig. S7D). Compared with neomycin group, *Pgc-1α* silencing increased the overlap co-efficiency of Bodipy(558/568)-C12 with LDs, accompanied by a significant decrease in the overlap between mitochondria and Bodipy(558/568)-C12. These findings indicated that neomycin can limit the turnover of LDs and the trafficking of FAs from LDs to mitochondria, and that PGC-1α deficiency obviously worsened the disturbance of lipid homeostasis and FA underuse. Bodipy(581/591)-C11, a probe for lipid peroxidation in living cells or membrane systems, showed that neomycin-induced oxidized C11 (green) signals were exacerbated in *Pgc-1α* deficient cells with the decay of non-oxidized C11 (red) signals (Fig. 6E, Fig. S7E). Consistently, MitoSOX analysis also supported the above data (Supporting Information Fig. S8). This suggested PGC-1α plays an important role in maintaining the interactions between LDs and mitochondria and the dynamic lipid homeostasis.

3.7. *Pgc-1α$^{-/-}$ exacerbates neomycin-induced toxicity and lipid disorders in the inner ear and kidney in vivo*

To further investigate whether PGC-1α plays a role in neomycin-induced toxicity and lipid disorders *in vivo*, PGC-1α whole body

KO mice were exposed to 100 mg/kg neomycin for 7 consecutive days (Fig. 7A, Supporting Information Fig. S9A and S9B). A dose of 200 mg/kg neomycin led to a 50% mortality rate in the exposed population, suggesting that KO mice were more sensitive to the toxicity of neomycin. Compared with those of WT mice, KO mice exhibited significantly elevated renal injury markers including serum creatinine, and gene expression levels of *Kim-1* and *Ngal*, after 7 days of neomycin administration (Fig. 7B). Pathological examination revealed more pronounced brush border disruption and tubular dilation, and the intensity and extent of the NGAL immunostaining progressively increased in the KO mice compared with the WT mice after 7 days of drug exposure. Transmission electron microscopy images also depicted more severe cristae disruption, mitochondrial swelling and LD accumulation in the KO mice (Fig. 7C).

Regarding hearing function assessment, ABR measurements indicated besides the injury at higher frequencies, KO mice also exhibited evident threshold elevations at 4, 8, 12, and 16 kHz after neomycin treatment for 7 days, suggesting more severe hearing dysfunction (Fig. 7D). And KO mice also suffered significant loss of hair cells at the basal turn of the cochleae (Fig. 7E). Drug distribution in the kidneys and inner ears by HPLC−MS/MS analysis showed that neomycin accumulation in both organs was significantly higher in *Pgc-1α* deficient mice than WT mice after 7 days of neomycin administration (Fig. S9C).

A lipidomic study confirmed that PGC-1α deficiency aggravated neomycin-induced lipid disorders in the inner ears and kidneys. Heatmaps also indicated that compared with that in the kidneys, TAG in the inner ears was more affected after neomycin treatment (Fig. 7F and G). Additionally, there was a significant increase in polyunsaturated lipids in KO mice compared to WT mice after neomycin treatment (Fig. 7H). These results suggested that PGC-1α deficiency promoted neomycin-induced renal dysfunction and hearing impairment characterized by profound lipid metabolic disorders.

4. Discussion

The present study reveals that during drug-induced ototoxicity and nephrotoxicity, the spatiotemporal accumulation characteristics of neomycin in cochlear hair cells and renal tubular epithelial cells are closely related to lipid metabolism disorders and selective LD deposition in these two target injured organs. Neomycin is enriched in mitochondria or around mitochondria, leading to tight membrane interactions between mitochondria and LDs. This interaction results in abnormal mitochondrial morphology, increased lipid ROS, and blocked transfer of fatty acids from LDs to mitochondria. Knockout of PGC-1α, a crucial regulator of mitochondrial function and energy metabolism, exacerbated the pathological interplay between LDs and mitochondria. This exacerbation further intensified neomycin-induced lipid oxidation and metabolic dysfunction, as depicted in Fig. 8. This shared pathological mechanism may underlie the organ damage observed in individuals with drug-induced ototoxicity and nephrotoxicity.

Drug-induced nephrotoxicity and ototoxicity (caused by AGs or platinum) are intricately linked to *in vivo* pharmacokinetic behavior[31]. The toxicity of AGs is directly proportional to their accumulation in the kidney and inner ear, particularly in the mitochondria of hair cells and renal tubular epithelial cells. Unfortunately, hearing impairment caused by AGs is irreversible even after discontinuation of the drug, whereas renal function tends to recover over time. Our findings suggest that there is a deficiency in eliminating neomycin from the inner ear. This is evident from the continuous increase in neomycin accumulation in hair cells even after withdrawal, while neomycin levels in the kidney, heart, and liver decreased by 67.8%, 99.5%, and 37.5% respectively. Previous studies have reported that administering 200 mg/kg neomycin to mice for 7 consecutive days starting at P8 resulted in significant hair cell loss at the apex, middle, and basal turns of the cochleae at P30[32]. This finding indicates that delayed effect of drug accumulation on hair cells is significant. Moreover, the cochlea's high-frequency region is particularly susceptible to damage, which aligns with the observed spatiotemporal distribution of NTR accumulation in the hair cells of the basal turns. However, the precise cellular transports and molecular regulatory mechanisms responsible for these spatiotemporal differences require further investigation.

Additionally, alterations in lipidomics and the deposition of LD demonstrate distinct and location-specific patterns in the kidneys and cochleae, resembling drug distribution. Our current research is the inaugural study to illustrate the shared alterations in lipid metabolism, specifically TAG and phospholipids (PG, PE, PC, and PA), in both nephrotoxicity and ototoxicity induced by neomycin. Similarly, some studies have also identified varying degrees of lipid alterations in kidney disease patients. In a mouse model of renal injury induced by ischemia-reperfusion, significant increases were observed in plasma acylcholine, PC, and PE, in addition to TAG[33,34]. Platinum-induced nephrotoxicity has been shown to disrupt lipid metabolism, as indicated by the accumulation of TAG, elevated levels of Cer and hexosylceramides (HexCer), as well as changes in phospholipids (PG, PC, PE, LPC)[35,36]. Patients with CKD exhibit significant increases in total free fatty acids, glycerolipids, and PG[37]. These studies provide evidence suggesting that lipid metabolism plays a critical role in the maintenance of renal function. However, there is limited research available regarding the association between lipid metabolism disorders and inner ear injury.

In the context of neomycin-induced nephrotoxicity and ototoxicity, both organs exhibited a notable increase in the quantity and intensity of changes in TAG and phospholipid components compared to those in other lipids. Specifically, there was a significant increase in 13 types of TAG, 14 types of PG, 5 types of PE, and 2 types of PC, which are essential constituents of LD structures. TAG, functioning as an energy reservoir, is stored within LDs with cholesterol esters. Excessive accumulation of TAG and LDs can contribute to intracellular oxidative stress, inflammation, mitochondrial damage, and the progression of kidney disease[38,39]. Excessive PG has also been demonstrated to induce mitochondrial fragmentation or the generation of substantial mitochondrial fragments in yeast[40]. In the context of lipid accumulation in renal tubular cells induced by a high-fat diet (HFD), the accumulation of phospholipids in lysosomes was observed to disrupt autophagic flux, resulting in kidney injury[41]. Furthermore, the elevation in phospholipids containing double bonds also facilitated lipid peroxidation. Unsaturated lipids contain fatty acids with one or more carbon−carbon double bonds, and these bonds are the site for the peroxidation reaction[42,43]. Our study indicated that the greater the abundance of unsaturated lipids was, the greater the susceptibility to lipid peroxidation was. Notably, LD accumulation is particularly pronounced in inner hair

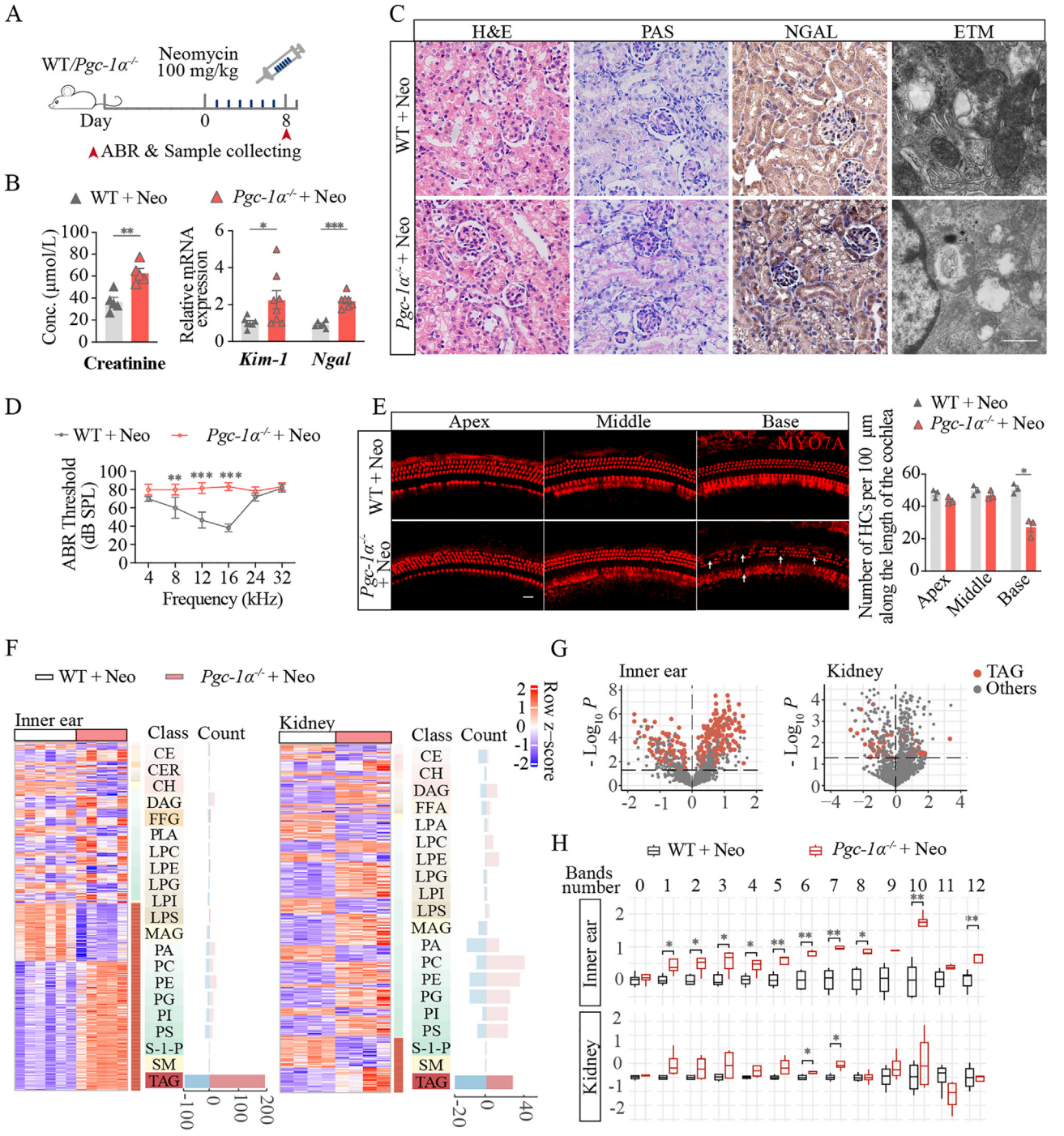

Figure 7 *Pgc-1α*$^{-/-}$ aggravated neomycin-induced toxicity and lipid metabolism disorder *in vivo*. (A) Schematic diagram of 100 mg/kg neomycin treatment for 7 consecutive days in mice. (B) Analysis of serum creatinine ($n = 5$), as well as relative RNA expression of renal tubular injury marker genes ($n = 7–8$). (C) Histological photomicrographs of kidney tissue sections stained with H&E, PAS, Scale bar = 50 μm; NGAL immunostaining of kidney tissue sections, Scale bar = 50 μm; Electron micrographs of mitochondria in kidney tubule. Scale bar = 2 μm. (D) ABR measurement of mice ($n = 3$). (E) Representative confocal images of hair cells and quantification of MYO7A$^+$ hair cells in three turns of cochleae ($n = 3$). Scale bar = 20 μm. (F) Heatmaps and counts of significantly changed lipids ($P < 0.05$) in inner ears and kidneys ($n = 4–6$). (G) Volcano plot illustrating significantly altered TAGs estimated by LC−MS. (H) Relative abundance for TAGs and PLs containing double bonds by LC−MS. Experiment groups: WT + Neo, WT mice treated with 100 mg/kg neomycin once daily subcutaneously for 7 consecutive days; *Pgc-1α*$^{-/-}$ +Neo, *Pgc-1α*$^{-/-}$ mice treated with 100 mg/kg neomycin once daily subcutaneously for 7 consecutive days. *Ngal*, neutrophil gelatinase-associated lipocalin; *Kim-1*, hepatitis A virus cellular receptor 1. The results are presented as the mean ± SEM. *$P < 0.05$, **$P < 0.01$, ***$P < 0.001$.

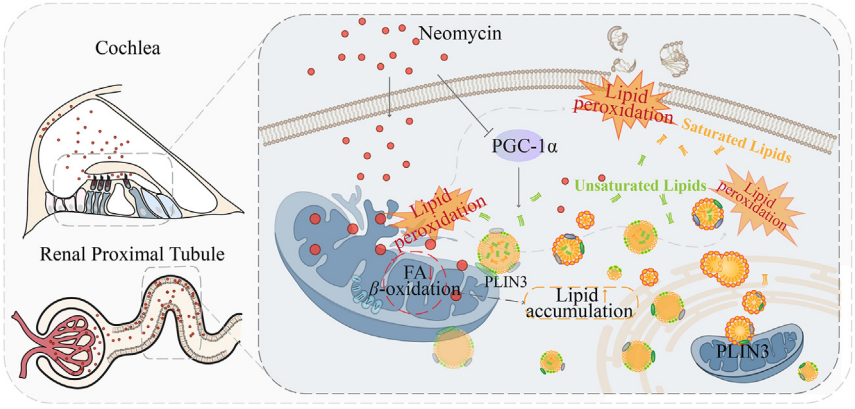

Figure 8 Schematic of neomycin-induced ototoxicity and nephrotoxicity. Neomycin targets mitochondria in hair cells and renal tubular epithelial cells, impairs mitochondrial function and disrupts lipid metabolism by promoting the interactions between LDs and mitochondria, as well as downregulating the expression of related genes, leading to the accumulation of LDs and unsaturated lipids. This, in turn, further caused mitochondrial dysfunction. As the managerial factor of mitochondrial function and lipid metabolism, PGC-1α plays an important role in regulating neomycin-induced ototoxicity and nephrotoxicity.

cells and supporting cells, which play a crucial role in transmitting auditory signals from the cochlea to the brain. Abnormal lipid accumulation in inner hair cells may affect the afferent of sound, ultimately leading to shifts in the ABR threshold.

Interestingly, our study revealed that NTR can induce membrane interactions between mitochondria and LDs, with abnormal mitochondrial morphology observed in the interaction structure. With the prolonged neomycin administration, the number and volume of LDs in ear and kidney cells increase significantly, and there are more and more LDs bound to mitochondria, which may lead to increased damage to mitochondrial structure. In recent years, a growing number of researches have confirmed the significant role of peridroplet mitochondria in regulating cellular energy metabolism and maintaining lipid homeostasis[44]. In response to stress, the interactions between LDs and mitochondria increases, allowing for more efficient transfer of fatty acids to mitochondria for cellular function, and limiting the dispersion of free fatty acids within cells to reduce their toxicity to cells.

However, our results showed that the transfer of fatty acids to mitochondria was blocked. Peridroplet mitochondria isolated from brown adipose tissue exhibited reduced β-oxidation capacity[45]. Compared with cytoplasmic mitochondria, peridroplet mitochondria isolated from HFD-induced NAFLD animals also exhibited decreased β-oxidation levels and LD accumulation[46]. Our study demonstrated that neomycin-induced intracellular damage to mitochondria led to abnormal cellular energy metabolism, increased LDs, enhanced interactions between LDs and mitochondria, and reduced β-oxidation levels. And the enhanced levels of oxidized lipids further exacerbated mitochondrial damage and promoted cell death. The mechanisms underlying lipid metabolic disorders and LD−mitochondria interactions in both kidneys and cochleae remain unclear.

The PLIN family comprises the most abundant LD coating proteins in mammalian cells; these proteins participate in the regulation of lipid metabolism and contribute to the modulation of interactions between LDs and mitochondria[47]. The distribution and functions of miRNAs vary depending on the specific tissues, cell types, and metabolic states. PLIN5, PLIN1, and PLIN2 are expressed mainly in various tissues such as adipose, muscle, liver, and heart, while PLIN3 is predominantly found in highly oxidative tissues like the heart and skeletal muscles. The functions and expression of the PLIN family in the inner ear have not been reported yet. The present study revealed that PLIN2 and PLIN3 levels increased in the kidney, and that PLIN3 levels increased in the inner ear after neomycin administration. Previous research indicated that PLIN2 was upregulated in mouse kidneys following I/R, resulting in the downregulation of PPARα and the apoptosis of renal tubular epithelial cells[48]. PLIN3 expression is associated with clear cell renal cell carcinoma and was part of the GATA1/miR-885-5p/PLIN3 pathway, which regulated the sensitivity of clear cell renal cell carcinoma to sunitinib[49]. Enhanced coupling of mitochondria and LDs mediated by PLIN5 increased myocardial cell respiration capacity and metabolic flexibility[50]. Therefore, the increased expression of PLIN2 and PLIN3 in neomycin-induced ear and kidney injuries may not only signify LD accumulation but could also involve the regulation of cellular signaling pathways and mediation of interactions between LDs and mitochondria. Their roles in ear and kidney injuries deserve further investigation.

PGC-1α plays a critical role in regulating mitochondrial function under stress conditions[51]. Knockout of PGC-1α in mice exacerbates mitochondrial and oxidative stress-induced kidney injuries caused by folic acid and LPS, as well as augmenting the apoptosis of auditory cells induced by gentamicin[52-54]. Consistent with the findings of previous reports, PGC-1α deficiency promoted hearing and kidney functional injuries and mitochondrial damage induced by neomycin, further underscoring the crucial role of PGC-1α in mediating drug-induced ear and kidney injuries. Moreover, PGC-1α silence exacerbated cellular lipid accumulation and peridroplet mitochondrial formation. It has been reported that PLIN5 formed a transcriptional nuclear complex with PGC-1α and Sirtuin 1 to PGC-1α function[55]. Currently, there are no relevant reports on the interactions between PGC-1α and PLIN3. Our experimental results demonstrated that PGC-1α knockout increases PLIN3 expression, suggesting a potential relationship between PGC-1α and PLIN3 in the regulation of lipid metabolism. Further research is needed to elucidate the specific signaling pathways involved. This study helps us better understand the molecular basis of LD homeostasis and their relationship to mitochondrial function.

5. Conclusions

There is a tissue-specific correlation between neomycin accumulation and LDs in combined ear and kidney injury induced by neomycin. Simultaneously, neomycin targets mitochondria, leading to disruption of lipid metabolism in the inner ear and kidney, causing LD accumulation and increased interactions between mitochondria and LDs. PGC-1$\alpha^{-/-}$ further exacerbated the imbalance of mitochondria-LD homeostasis, intensified cellular lipid peroxidation, and worsened cellular injury, suggesting that regulating PGC-1α-mediated mitochondria-LD homeostasis may be a potential strategy for drug-induced ear and kidney injuries.

Acknowledgments

This study was supported by the National Natural Science Foundation of China (82274014, 82330033, 82030029, 92149304, 82101228), the Leading Technology Foundation Research Project of Jiangsu Province (BK20192005, China), National Key R&D Program of China (Nos. 2021YFA1101300, 2021YFA1101800, and 2020YFA0112503), the Project of State Key Laboratory of Natural Medicines, China Pharmaceutical University (SKLNMZZ202302, China). The authors express gratitude to Prof. Yiwen Zheng from University of Otago, New Zealand, for her generous guidance on mice cochlear explants culture. Special thanks to Guangzhou CSR Biotech Co., Ltd. for live-cell imaging by their commercial super-resolution structured illumination microscope HIS-SIM for data acquisition, SR image reconstruction.

Author contributions

Bin Chen: Writing − review & editing, Writing − original draft, Visualization, Validation, Software, Methodology, Investigation, Formal analysis, Data curation, Conceptualization. Cheng Cheng: Project administration, Methodology, Investigation, Data curation, Conceptualization. Yunhao Wu: Methodology, Investigation, Formal analysis, Data curation, Conceptualization. Siyu Li: Visualization, Validation, Methodology, Investigation, Data curation, Conceptualization. Mo Han: Visualization, Methodology, Data curation. Le Zhen: Methodology. Ying Peng: Software, Data curation. Suhan Guo: Methodology. Kaidi Shen: Methodology. Xia Gao: Validation. Renjie Chai: Writing − review & editing, Validation, Supervision, Resources, Project administration, Methodology, Investigation, Funding acquisition, Conceptualization. Guangji Wang: Writing − review & editing, Validation, Supervision, Resources, Project administration, Investigation, Funding acquisition, Conceptualization. Fang Zhou: Writing − review & editing, Writing − original draft, Visualization, Validation, Supervision, Resources, Project administration, Methodology, Investigation, Funding acquisition, Formal analysis, Data curation, Conceptualization.

Conflicts of interest

The authors declare no conflicts of interest.

Appendix A. Supporting information

Supporting information to this article can be found online at https://doi.org/10.1016/j.apsb.2024.05.024.

References

1. Bazzi C, Venturini CT, Pagani C, Arrigo G, D'Amico G. Hearing loss in short- and long-term haemodialysed patients. *Nephrol Dial Transpl* 1995;**10**:1865−8.
2. Jamaldeen J, Basheer A, Sarma AC, Kandasamy R. Prevalence and patterns of hearing loss among chronic kidney disease patients undergoing haemodialysis. *Australas Med J* 2015;**8**:41−6.
3. Shim YJ, Choi HG, Wee JH. Association between chronic kidney disease and sudden sensorineural hearing loss: a longitudinal follow-up studies using ICD-10 codes in a national health screening cohort. *J Clin Med* 2023;**12**:2861.
4. Wang H, Zhu B. *Basic theories of traditional Chinese medicine*. London: Jessica Kingsley Publishers; 2011.
5. Phelan PJ, Rheault MN. Hearing loss and renal syndromes. *Pediatr Nephrol* 2018;**33**:1671−83.
6. Verdel BM, van Puijenbroek EP, Souverein PC, Leufkens HG, Egberts AC. Drug-related nephrotoxic and ototoxic reactions: a link through a predictive mechanistic commonality. *Drug Saf* 2008;**31**:877−84.
7. Falagas ME, Matthaiou DK, Bliziotis IA. The role of aminoglycosides in combination with a beta-lactam for the treatment of bacterial endocarditis: a meta-analysis of comparative trials. *J Antimicrob Chemother* 2006;**57**:639−47.
8. Gonzalez 3rd LS, Spencer JP. Aminoglycosides: a practical review. *Am Fam Physician* 1998;**58**:1811−20.
9. Drusano GL, Louie A. Optimization of aminoglycoside therapy. *Antimicrob Agents Chemother* 2011;**55**:2528−31.
10. Yao L, Zhang JW, Chen B, Cai MM, Feng D, Wang QZ, et al. Mechanisms and pharmacokinetic/pharmacodynamic profiles underlying the low nephrotoxicity and ototoxicity of etimicin. *Acta Pharmacol Sin* 2020;**41**:866−78.
11. Wang X, Zhu H, Hu J, Li H, Guo S, Chen B, et al. Magnesium isoglycyrrhizinate reduces the target-binding amount of cisplatin to mitochondrial DNA and renal injury through SIRT3. *Int J Mol Sci* 2022;**23**:13093.
12. He Y, Zheng Z, Liu C, Li W, Zhao L, Nie G, et al. Inhibiting DNA methylation alleviates cisplatin-induced hearing loss by decreasing oxidative stress-induced mitochondria-dependent apoptosis *via* the LRP1−PI3K/AKT pathway. *Acta Pharm Sin B* 2022;**12**:1305−21.
13. Nan B, Zhao Z, Jiang K, Gu X, Li H, Huang X. Astaxanthine attenuates cisplatin ototoxicity *in vitro* and protects against cisplatin-induced hearing loss *in vivo*. *Acta Pharm Sin B* 2022;**12**:167−81.
14. McQuate A, Knecht S, Raible DW. Activity regulates a cell type-specific mitochondrial phenotype in zebrafish lateral line hair cells. *Elife* 2023;**12**:e80468.
15. Duann P, Lin PH. Mitochondria damage and kidney disease. *Adv Exp Med Biol* 2017;**982**:529−51.
16. Houten SM, Violante S, Ventura FV, Wanders RJ. The biochemistry and physiology of mitochondrial fatty acid beta-oxidation and its genetic disorders. *Annu Rev Physiol* 2016;**78**:23−44.
17. Srivastava A, Srivastava P, Mathur S, Abbas S, Rai N, Tiwari S, et al. Lipid metabolism and mitochondria: cross talk in cancer. *Curr Drug Targets* 2022;**23**:606−27.
18. Zhao Q, Zhou X, Kuiper R, Curbo S, Karlsson A. Mitochondrial dysfunction is associated with lipid metabolism disorder and upregulation of angiotensin-converting enzyme 2. *PLoS One* 2022;**17**:e0270418.
19. Shen Y, Chen W, Han L, Bian Q, Fan J, Cao Z, et al. VEGF-B antibody and interleukin-22 fusion protein ameliorates diabetic nephropathy through inhibiting lipid accumulation and inflammatory responses. *Acta Pharm Sin B* 2021;**11**:127−42.
20. Xu S, Jia P, Fang Y, Jin J, Sun Z, Zhou W, et al. Nuclear farnesoid X receptor attenuates acute kidney injury through fatty acid oxidation. *Kidney Int* 2022;**101**:987−1002.

21. Sun Y, Ge X, Li X, He J, Wei X, Du J, et al. High-fat diet promotes renal injury by inducing oxidative stress and mitochondrial dysfunction. *Cell Death Dis* 2020;**11**:914.
22. Doosti A, Lotfi Y, Bakhshi E. Effects of hyperlipidemia on noise induced hearing loss (NIHL). *Indian J Otolaryngol Head Neck Surg* 2016;**68**:211−3.
23. Li X, Chen B, Zhou X, Ye F, Wang Y, Hu W. Identification of dyslipidemia as a risk factor for sudden sensorineural hearing loss: a multicenter case-control study. *J Clin Lab Anal* 2021;**35**: e24067.
24. Wu Q, Zhao M, He X, Xue R, Li D, Yu X, et al. Acetylcholine reduces palmitate-induced cardiomyocyte apoptosis by promoting lipid droplet lipolysis and perilipin 5-mediated lipid droplet−mitochondria interaction. *Cell Cycle* 2021;**20**:1890−906.
25. Wang J, Menchenton T, Yin S, Yu Z, Bance M, Morris DP, et al. Overexpression of X-linked inhibitor of apoptosis protein slows presbycusis in C57BL/6J mice. *Neurobiol Aging* 2010;**31**:1238−49.
26. Lin SCY, Thorne PR, Housley GD, Vlajkovic SM. Resistance to neomycin ototoxicity in the extreme basal (hook) region of the mouse cochlea. *Histochem Cell Biol* 2018;**150**:281−9.
27. Diez C, Guillarme D, Staub Sporri A, Cognard E, Ortelli D, Edder P, et al. Aminoglycoside analysis in food of animal origin with a zwitterionic stationary phase and liquid chromatography−tandem mass spectrometry. *Anal Chim Acta* 2015;**882**:127−39.
28. Herker E, Vieyres G, Beller M, Krahmer N, Bohnert M. Lipid droplet contact sites in health and disease. *Trends Cell Biol* 2021;**31**:345−58.
29. Wang H, Sreenivasan U, Hu H, Saladino A, Polster BM, Lund LM, et al. Perilipin 5, a lipid droplet-associated protein, provides physical and metabolic linkage to mitochondria. *J Lipid Res* 2011;**52**:2159−68.
30. Bour A, Kruglik SG, Chabanon M, Rangamani P, Puff N, Bonneau S. Lipid unsaturation properties govern the sensitivity of membranes to photoinduced oxidative stress. *Biophys J* 2019;**116**:910−20.
31. Steyger PS. Mechanisms of aminoglycoside- and cisplatin-induced ototoxicity. *Am J Audiol* 2021;**30**:887−900.
32. Zhang Y, Li W, He Z, Wang Y, Shao B, Cheng C, et al. Pre-treatment with fasudil prevents neomycin-induced hair cell damage by reducing the accumulation of reactive oxygen species. *Front Mol Neurosci* 2019;**12**:264.
33. Rao S, Walters KB, Wilson L, Chen B, Bolisetty S, Graves D, et al. Early lipid changes in acute kidney injury using SWATH lipidomics coupled with MALDI tissue imaging. *Am J Physiol Ren Physiol* 2016; **310**:F1136−47.
34. Ma H, Guo X, Cui S, Wu Y, Zhang Y, Shen X, et al. Dephosphorylation of AMP-activated protein kinase exacerbates ischemia/reperfusion-induced acute kidney injury *via* mitochondrial dysfunction. *Kidney Int* 2022;**101**:315−30.
35. Moreno-Gordaliza E, Marazuela MD, Pastor O, Lazaro A, Gomez-Gomez MM. Lipidomics reveals cisplatin-induced renal lipid alterations during acute kidney injury and their attenuation by cilastatin. *Int J Mol Sci* 2021;**22**:12521.
36. Moreno-Gordaliza E, Esteban-Fernandez D, Lazaro A, Humanes B, Aboulmagd S, Tejedor A, et al. MALDI-LTQ-Orbitrap mass spectrometry imaging for lipidomic analysis in kidney under cisplatin chemotherapy. *Talanta* 2017;**164**:16−26.
37. Chen H, Chen L, Liu D, Chen DQ, Vaziri ND, Yu XY, et al. Combined clinical phenotype and lipidomic analysis reveals the impact of chronic kidney disease on lipid metabolism. *J Proteome Res* 2017;**16**: 1566−78.
38. Bobulescu IA. Renal lipid metabolism and lipotoxicity. *Curr Opin Nephrol Hypertens* 2010;**19**:393−402.
39. Fornoni A, Merscher S. Lipid metabolism gets in a JAML during kidney disease. *Cell Metab* 2020;**32**:903−5.
40. Pokorna L, Cermakova P, Horvath A, Baile MG, Claypool SM, Griac P, et al. Specific degradation of phosphatidylglycerol is necessary for proper mitochondrial morphology and function. *Biochim Biophys Acta* 2016;**1857**:34−45.
41. Yamamoto T, Takabatake Y, Takahashi A, Kimura T, Namba T, Matsuda J, et al. High-fat diet-induced lysosomal dysfunction and impaired autophagic flux contribute to lipotoxicity in the kidney. *J Am Soc Nephrol* 2017;**28**:1534−51.
42. Papsdorf K, Miklas JW, Hosseini A, Cabruja M, Morrow CS, Savini M, et al. Lipid droplets and peroxisomes are co-regulated to drive lifespan extension in response to mono-unsaturated fatty acids. *Nat Cell Biol* 2023;**25**:672−84.
43. Fu Y, He Y, Phan K, Bhatia S, Pickford R, Wu P, et al. Increased unsaturated lipids underlie lipid peroxidation in synucleinopathy brain. *Acta Neuropathol Commun* 2022;**10**:165.
44. Eynaudi A, Diaz-Castro F, Borquez JC, Bravo-Sagua R, Parra V, Troncoso R. Differential effects of oleic and palmitic acids on lipid droplet−mitochondria interaction in the hepatic cell line HepG2. *Front Nutr* 2021;**8**:775382.
45. Benador IY, Veliova M, Mahdaviani K, Petcherski A, Wikstrom JD, Assali EA, et al. Mitochondria bound to lipid droplets have unique bioenergetics, composition, and dynamics that support lipid droplet expansion. *Cell Metab* 2018;**27**:869−885. e6.
46. Talari NK, Mattam U, Meher NK, Paripati AK, Mahadev K, Krishnamoorthy T, et al. Lipid-droplet associated mitochondria promote fatty-acid oxidation through a distinct bioenergetic pattern in male Wistar rats. *Nat Commun* 2023;**14**:766.
47. Ajjaji D, Ben M, barek K, Mimmack ML, England C, Herscovitz H, et al. Dual binding motifs underpin the hierarchical association of perilipins1−3 with lipid droplets. *Mol Biol Cell* 2019;**30**:703−16.
48. Xu S, Lee E, Sun Z, Wang X, Ren T, Zou Z, et al. Perilipin 2 impacts acute kidney injury *via* regulation of PPARα. *J Immunol Res* 2021; **2021**:9972704.
49. Yao D, Xia S, Jin C, Zhao W, Lan W, Liu Z, et al. Feedback activation of GATA1/miR-885-5p/PLIN3 pathway decreases sunitinib sensitivity in clear cell renal cell carcinoma. *Cell Cycle* 2020;**19**:2195−206.
50. Kien B, Kolleritsch S, Kunowska N, Heier C, Chalhoub G, Tilp A, et al. Lipid droplet-mitochondria coupling *via* perilipin 5 augments respiratory capacity but is dispensable for FA oxidation. *J Lipid Res* 2022;**63**:100172.
51. Adhihetty PJ, Uguccioni G, Leick L, Hidalgo J, Pilegaard H, Hood DA. The role of PGC-1α on mitochondrial function and apoptotic susceptibility in muscle. *Am J Physiol Cell Physiol* 2009; **297**:C217−25.
52. Fontecha-Barriuso M, Martin-Sanchez D, Martinez-Moreno JM, Carrasco S, Ruiz-Andres O, Monsalve M, et al. PGC-1α deficiency causes spontaneous kidney inflammation and increases the severity of nephrotoxic AKI. *J Pathol* 2019;**249**:65−78.
53. Tran M, Tam D, Bardia A, Bhasin M, Rowe GC, Kher A, et al. PGC-1α promotes recovery after acute kidney injury during systemic inflammation in mice. *J Clin Invest* 2011;**121**:4003−14.
54. Han H, Dong Y, Ma X. Dihydromyricetin protects against gentamicin-induced ototoxicity *via* PGC-1α/SIRT3 signaling *in vitro*. *Front Cell Dev Biol* 2020;**8**:702.
55. Gallardo-Montejano VI, Saxena G, Kusminski CM, Yang C, McAfee JL, Hahner L, et al. Nuclear Perilipin 5 integrates lipid droplet lipolysis with PGC-1α/SIRT1-dependent transcriptional regulation of mitochondrial function. *Nat Commun* 2016;**7**:12723.